BIOCHEMISTRY
including biophysical chemistry & molecular biology
Article

Biochemistry **2010,** *49,* 8857–8872 8857
DOI: 10.1021/bi100499a

Unprecedented Peroxidase-like Activity of *Rhodnius prolixus* Nitrophorin 2: Identification of the [Fe^{IV}=O $Por^{\bullet}$]$^{+}$ and [Fe^{IV}=O Por]($Tyr38^{\bullet}$) Intermediates and Their Role(s) in Substrate Oxidation[†]

Rahul Singh,[‡] Robert E. Berry,[§] Fei Yang,[§] Hongjun Zhang,[§] F. Ann Walker,*[,§] and Anabella Ivancich*[,‡]

[‡]*CNRS URA 2096. CEA, iBiTec-S, Laboratoire des Hyperfréquences, Métalloprotéines et Systèmes de Spin, F-91191 Gif-sur-Yvette, France, and* [§]*Department of Chemistry and Biochemistry, The University of Arizona, Tucson, Arizona 85721-0041*

Received April 2, 2010; Revised Manuscript Received August 18, 2010

ABSTRACT: We have identified a novel enzymatic reaction for nitrophorin 2 (NP2), a heme protein previously characterized as a nitric oxide carrier in the saliva of the *Rhodnius prolixus* insect. NP2 exhibited levels of peroxidase activity comparable to those of the bifunctional peroxidases (KatGs), despite their heme pocket structural differences (heme ruffling, Tyr38 and Tyr85 in hydrogen bonding interactions with the propionates in NP2). The intermediates of the peroxidase-like reaction of NP2 were identified by Electron Paramagnetic Resonance (EPR) and electronic absorption spectroscopies. The EPR spectrum consistent with an [Fe^{IV}=O $Por^{\bullet}$]$^{+}$ species was detected at pH <7. At pH ≥ 7, the change from a strong to a weak antiferromagnetic coupling interaction for the [Fe^{IV}=O $Por^{\bullet}$]$^{+}$ species was accompanied by the subsequent formation of an [Fe^{IV}=O Por]($Tyr^{\bullet}$) intermediate. Tyr38 was shown to be the unique naturally occurring radical site in NP2. The Y38F mutant stabilized the radical on the tyrosine in hydrogen-bonding interaction with the other heme propionate (Tyr85). Kinetic studies using stopped-flow electronic absorption spectrophotometry revealed that the [Fe^{IV}=O $Por^{\bullet}$]$^{+}$ species reacts with histamine and norepinephrine in a peroxidase-like manner. Our findings demonstrate that NP2 has pH-dependent dual function: at the acidic pH of the insect saliva the protein behaves as a NO carrier, and, if exposed to the higher pH of the tissues and capillaries of the host, NP2 is able to bind histamine or it can efficiently inactivate norepinephrine through a peroxidase-like reaction, in the presence of hydrogen peroxide. Accordingly, the unprecedented peroxidase-like activity of NP2 is concluded to be a key biological function.

There are few examples of heme proteins capable of accomplishing enzymatic reactions at catalytically competent rates when their heme microenvironments differ substantially from those of the enzymes specifically tuned for the given reaction. An interesting example is that of the bifunctional heme peroxidases, also known as catalase-peroxidases (KatGs), which can perform the disproportionation of hydrogen peroxide at rates comparable to those of monofunctional catalases, although the heme active site and the overall three-dimensional structure resemble those of a peroxidase (*1*−*3*). Prostaglandin H synthase (PGHS), a membrane-bound bifunctional heme protein having two isoforms that play a key role in the biosynthesis of prostaglandins and thromboxanes, is another example of a protein with dual enzymatic activity (reviewed in ref *4*). PGHS catalyzes the conversion of arachidonic acid to prostaglandin G2 via a cyclooxygenase-type activity and the subsequent two-electron reduction of prostaglandin G2 to prostaglandin H2 via a peroxidase-type cycle. An additional finding that provides renewed interest in KatGs and PGHS is the fact that protein-based radicals are formed by intramolecular electron transfer between specific Tyr or Trp residues and the heme. These radicals act as alternative reactive intermediates to the [Fe^{IV}=O $Por^{\bullet}$]$^{+}$ species in the catalytic cycles. In particular, it has been shown that the [Fe^{IV}=O Por]($Tyr^{\bullet}$) intermediate formed on Tyr385 of PGHS is responsible for the reaction with arachidonic acid (*4*), and that the [Fe^{IV}=O Por]($Trp^{\bullet}$) intermediate of *Mycobacterium tuberculosis* catalase-peroxidase is the reactive species that activates the prodrug isoniazid (*5*). Also, it has recently been proposed that a radical on the cross-linked Met-Tyr-Trp triad of *M. tuberculosis* KatG is required for catalase activity (*6*).

It is relevant to explore putative peroxidase-like reactions in other heme proteins, including the nitrophorins of interest in this work, and to characterize the electronic structures of the reactive intermediates in relation to their function. Nitrophorins (NPs) constitute a group of heme proteins present in the saliva of the blood-sucking insect *Rhodnius prolixus*. NPs have been shown to be essential as nitric oxide (NO) storage and delivery systems (*7*−*10*). The ferriheme active site is finely tuned to allow transport of NO to the host tissues and capillaries, followed by NO release. Histamine, a substance released from platelets and mast cells of the host in response to the insect's bite, is then bound to the NPs (*7*, *8*). Accordingly, the release of NO improves the blood flow due to the vasodilator and blood anticoagulation effects, while the binding of histamine to NPs prevents detection of the insect by the host (*7*−*10*). The pH dependence of the equilibrium constant for the release of NO from the ferriheme iron of

[†]This work was supported by the French National Research Council (CNRS), the French Atomic Energy Commission (CEA-Saclay) (A.I.), and National Science Foundation Grant CHE-0809591 (F.A.W.). R.S. acknowledges a postdoctoral fellowship from CEA-Saclay.

*To whom correspondence should be addressed. F.A.W.: Department of Chemistry and Biochemistry, The University of Arizona, Tucson, AZ 85721-0041; phone, (520) 621-8645; fax, (520) 626-9300; e-mail, awalker@email.arizona.edu. A.I.: Centre d'Etudes de Saclay, iBiTec-S, SB2SM, Bat 532, F-91191 Gif-sur-Yvette, France; phone, +33 1 69088717; fax, +33 1 69082842; e-mail, anabella.ivancich@cea.fr.

© 2010 American Chemical Society
Published on Web 08/20/2010

nitrophorin 2 (NP2)[1] shows that the K_d is ~3-fold smaller at the acidic pH of the insect's saliva (pH 5.5) than at the near-neutral pH of the host tissue (pH 7.35); likewise, the rate constant for NO release, k_d, is also ~3-fold lower at acidic pH than at near-neutral pH (R. E. Berry, unpublished results). Such a pH-dependent selectivity for release of NO (and binding of histamine) favors a more efficient blood uptake by the insect.

The crystal structure of NP2 shows that the active site is a six-coordinate ferriheme center with His57 as the protein-provided ligand and a NH_3 molecule, supplied by the $(NH_4)_2HPO_4$ crystallization buffer (pH 7.7), or a water molecule at lower pH (6.5) as the sixth ligand (*11*, *12*). The EPR spectrum of NP2 in the absence of NO is characteristic of heme iron in the ferric high-spin state (*13*). Moreover, the distal side of the heme in the absence of NO shows a very unique configuration, with ordered water molecules hydrogen-bonded to the bound NH_3 or H_2O as well as leucine residues that are believed to cause specific ruffling of the heme (*11*, *12*, *14*−*20*); such ruffling is unusual in other heme proteins such as hemoglobins, myoglobins, peroxidases, KatGs, and catalases. Another interesting difference between NP2 and peroxidases, KatGs, and catalases is the presence of two Tyr residues (Tyr38 and Tyr85) within hydrogen bonding distance of the heme propionates. Specifically, the distance between the phenolic oxygen of Tyr38 and the carboxylate oxygen of the 7-propionate is 2.78 Å. In the case of Tyr85, the interaction with the other heme propionate involves a bridging water molecule; the distances between the phenolic oxygen and water244 and between water244 and the carboxylate oxygen of the heme 6-propionate are 2.61 and 2.72 Å, respectively (*11*, *12*). It has been shown that a single mutation of Tyr38 to alanine induces significant changes in the midpoint potential of the Fe^{III}/Fe^{II} couple (40 and 60 mV at pH 5.5 and 7.5, respectively), while mutation of Tyr85 to alanine induces smaller changes (−20 and 20 mV at pH 5.5 and 7.5, respectively) (R. E. Berry, A. Amoia, A. Weichsel, T. K. Shokhireva, M. N. Shokhirev, W. J. Golden, H. Zhang, W. R. Montfort, and F. A. Walker, manuscript to be submitted).

In a previous study that was aimed at determining whether nitrosothiols (RSNO) could be produced from the NO-loaded NPs and thiols (RSH), Ribeiro found that the reaction of the NO-loaded nitrophorins with cysteine caused destruction of the NO, and a slow thiol oxidase reaction occurred producing cystine (the oxidized, disulfide-bridged dimer of cysteine) and hydrogen peroxide occurred (*21*). Thus, hydrogen peroxide may be created in the tissues of the victim by the nitrophorins. In addition, it has been shown that there are micromolar levels of hydrogen peroxide in human blood plasma (*22*). The findings of Ribeiro on the production of hydrogen peroxide in human tissues (*21*) led to a subsequent preliminary study of the oxygenase activity of NP2 (*23*), in which it was concluded that the reaction of NO-free NP2 with norepinephrine in the presence of hydrogen peroxide was due to a peroxidase-like reaction of the protein. The "destruction" of norepinephrine, as well as that of the heme active site of NP2, were reported to be the products of such a reaction (*23*). Heme degradation was inferred from the severe bleaching of the Soret band in the electronic absorption spectrum of NP2 after the reaction with hydrogen peroxide and norepinephrine. Such an effect, which may possibly have been induced by a large excess of hydrogen peroxide, is certainly unexpected for a heme protein with relevant peroxidase-like activity. Also, such a peroxidase reaction of NP2 would not be anticipated if one considers the substantial differences in the heme pocket in NP2, in particular on the heme distal side, as compared to typical peroxidases.

Accordingly, a detailed characterization of the putative peroxidase-like reactivity of NP2 under well-controlled conditions, as well as the protein's reaction with peroxide and norepinephrine, was required to address the question of whether a significant peroxidase-like reaction might be competitive with the main protein functions of the nitrophorins, i.e., those of pH-dependent NO binding and release and histamine binding (*7*−*10*). A better understanding of the molecular mechanism of the putative reaction of NP2 with norepinephrine, a substance released tonically from sympathetic nerve endings in the skin and known to constrict blood vessels, could also shine light on the physiological implications of this reaction.

In this work, we have investigated the putative peroxidase-like activity of NP2 by using EPR spectroscopy and stopped-flow UV−vis electronic absorption spectrometry. The intermediates in the reaction of NP2 with hydrogen peroxide and peroxyacetic acid were thoroughly characterized, as was their reactivity with benzohydroxamic acid, norepinephrine, and histamine as substrates. The complementary information obtained from EPR and stopped-flow studies allowed us to discriminate three intermediates upon reaction of the NP2 with peroxyacetic acid, i.e., $[Fe^{IV}{=}O\ Por^{\bullet}]^+$, $[Fe^{IV}{=}O\ Por](Tyr^{\bullet})$, and $[Fe^{IV}{=}O\ Por]$ (Compound II), the equilibrium concentrations of which were clearly pH-dependent. The 9 GHz EPR characterization of the intermediates allowed us to discern an unusual pH-dependent effect on the $[Fe^{IV}{=}O\ Por^{\bullet}]^+$ species. At pH ≥7, the EPR spectrum agrees well with a weakly ferromagnetically coupled signal, typical of peroxidases, which became strongly ferromagnetically coupled to the ferryl iron at pH < 7. Such a strong ferromagnetic coupling interaction has been reported previously only in the case of heme model complexes that have *meso* substituents (*24*−*27*). As peroxidases, the $[Fe^{IV}{=}O\ Por^{\bullet}]^+$ intermediate of NP2 was shown to be the reactive species with BHA, histamine, and norepinephrine. In addition, EPR spectroscopy combined with site-directed mutagenesis allowed us to identify Tyr38, the Tyr residue in H-bonding interaction with the carboxyl group of the heme 7-propionate, as the radical site of the $[Fe^{IV}{=}O\ Por](Tyr^{\bullet})$ intermediate. The latter was formed subsequently to the $[Fe^{IV}{=}O\ Por^{\bullet}]^+$ species, and exclusively at pH ≥7. The EPR characterization of the Y38F, Y85F, and Y38F/Y85F mutants of NP2 showed that when Tyr38 was suppressed, the sole alternative radical site was Tyr85, despite the existence of eight other tyrosines (and a tryptophan) in NP2. In the crystal structures, Tyr85 is in a hydrogen bond interaction with the heme 6-propionate via a structural water (see Figure 2 below). The biological implications of the peroxidase-like

[1]Abbreviations: NP2, nitrophorin 2; EPR, electron paramagnetic resonance; NMR, nuclear magnetic resonance; SVD, singular-value decomposition; BHA, benzohydroxamic acid; ABTS, 2,2′-azinobis-(3-ethylbenzthiazoline-6-sulfonic acid); *o*-dianisidine, 3,3′-dimethoxybenzidine; ferryl, PAA, peroxyacetic acid; $(Fe^{IV}{=}O)^{2+}$; Compound I, reactive iron porphyrin species created by two-electron oxidation of ferric heme centers by reaction with hydrogen peroxide or its equivalents (organic peroxides or O_2 with two electrons and two protons); π-cation radical, incomplete description of the "ferryl porphyrin cation radical," in which $(Fe^{IV}{=}O)^{2+}$, a cation, is complexed to a one-electron-oxidized porphyrin anion, $Por^{\bullet-}$ (where an electron has been removed from a porphyrin π-orbital), to create a high-valent iron porphyrin species, $[Fe^{IV}{=}O\ Por^{\bullet}]^+$, which is an overall cation [other species of the same two-electron-oxidized state can be created by intramolecular transfer of an electron from a protein side chain to the porphyrin radical, the $[Fe^{IV}{=}O\ Por](Trp^{\bullet})$ or $[Fe^{IV}{=}O\ Por](Tyr^{\bullet})$ intermediate]; Compound II, reactive ferryl porphyrin species usually formulated as $[Fe^{IV}{=}O\ Por]$, which is created by one-electron reduction of Compound I without creation of a protein radical, or by one-electron chemical oxidation of a ferric porphyrin in the presence of an oxo-producing species.

reaction of ferric NP2 with norepinephrine, with respect to the mechanism of NO and histamine binding, are discussed.

MATERIALS AND METHODS

Sample Preparation. The radical species of the Fe(tmtmp) triflate model heme complex was obtained as previously described (*28*). Nitrophorin 2 was purified as previously described (*29*, *30*). Standard genetic engineering methods were employed to produce the various target nitrophorin gene mutants in the pET24a (Novagen) expression plasmids and were confirmed by sequencing. The *Escherichia coli*-expressed proteins were purified as described previously (*29*, *30*) and were preliminarily characterized by UV−visible spectroscopy and by mass spectrometry using MALDI-TOF (matrix assisted laser desorption ionization time of flight) and/or electrospray. The proteins were stored in lyophilized form at −80 °C until they were used. Protein concentrations were determined by using the extinction coefficient of 1.5×10^5 M^{-1} cm^{-1} at 412 nm (*31*). BHA, ABTS, histamine, and norepinephrine were purchased from Sigma-Aldrich. To avoid the substantial changes in pH of phosphate buffer upon freezing, we used Tris-maleate buffer (50 mM) for all the experiments, which covered a wide pH range (5.2−8.6). Buffer was exchanged using centricon Y10 microconcentrators (Amicon).

Peroxidase Activity Measurements. Activity measurements were monitored with a UVIKON 922 (Kontron, St. Quentin-en-Yvelines, France) spectrophotometer, equipped with temperature-controlled cell holders and a water circulating bath (Minichiller). Peroxidase activity was determined spectrophotometrically using ABTS (ε_{405} = 36.8 mM^{-1} cm^{-1}) and *o*-dianisidine (ε_{460} = 11.3 mM^{-1} cm^{-1}) as electron donors and H_2O_2 or PAA as the reactant. The reactions were performed in a 1 mL final volume in a 1 cm path length cuvette via addition of appropriately diluted NP2 (1−5 μL of enzyme at a concentration of 9 μM) in 50 mM Tris-maleate at the desired pH. One unit of peroxidase is defined as the amount that decomposes 1 μmol of electron donor in 1 min in a solution of 0.4 mM ABTS or 0.36 mM *o*-dianisidine and 2.5 mM H_2O_2 or PAA at 25 °C. The optimum pH for the peroxidase activity was determined by measuring the specific activity over a range of pH values from 4 to 9 using ABTS. Initial velocities were determined across the range of ABTS concentrations while the reactant (H_2O_2 or PAA) was kept constant, as well as across the range of reactant concentrations while the ABTS concentration was kept constant. The initial velocities were fit to the Michaelis−Menten equation using a nonlinear regression analysis to determine apparent kinetic constants. The activity measurements on MtKatG and BpKatG were taken as previously described (*1*). No detectable levels of catalase activity could be detected for nitrophorin.

EPR Spectroscopy. The 9 GHz EPR spectra were recorded on a Bruker ER500 spectrometer equipped with a standard TE_{102} cavity, a liquid helium cryostat (Oxford Instruments), and a microwave frequency counter (Bruker ER049X). Initial protein concentrations of 0.5 mM were used for recording the 9 GHz EPR spectra. Typically, the samples were prepared by mixing manually the nitrophorin (50 mM Tris-maleate buffer at pH 5.2, 6.0, 7.0, and 8.0) with an equal volume of a 3-fold excess buffered peroxyacetic acid solution, directly into the 4 mm EPR tubes kept in ice. The reaction was stopped by rapid immersion of the EPR tube in liquid nitrogen after 2 s. Final concentrations (after the reaction) in the samples used in Figures 1−4 were 0.25 mM for the protein and 0.75 mM for PAA. For the experiments involving the reaction with substrates, the protein sample was preincubated with the substrate for 10 min at room temperature, prior to reaction with H_2O_2 or peroxyacetic acid, described above. The EPR spectrum of the native protein was recorded before and after incubation with the substrates (norepinephrine, ABTS, and BHA) to monitor putative spectral changes in the ferric EPR spectrum related to substrate binding.

Stopped-Flow UV−Vis Absorption Measurements. Time-dependent absorption spectra were recorded using a four-syringe SX20 stopped-flow spectrophotometer (Applied PhotoPhysics Ltd.) equipped for conventional dual mixing and sequential mixing stopped-flow measurements with an attached diode array detector. A refrigerated bath was used to regulate the temperature of the samples in the syringes and in the mixing cell. Measurements were taken at 5 and 20 °C. Typically, for the dual-mixing experiments, NP2 samples were used at an initial concentration of 10 μM and were mixed with an equal volume of peroxyacetic acid or hydrogen peroxide. Final concentrations (after mixing) were 5 μM protein and 10 μM PAA or 2 mM H_2O_2. In the sequential mixing experiments, the starting protein concentration was 20 μM, yielding the same final protein concentration. Data analysis was conducted using singular-value decomposition (SVD) in Pro-K.2000 Global Analysis (Applied PhotoPhysics Ltd.) to obtain the transition rate constants (k_n) between intermediates.

RESULTS

Activity Measurements. The peroxidase-like activity of NP2 was investigated over a pH range from 4.5 to 8.5 using hydrogen peroxide and peroxyacetic acid as reactants and ABTS or *o*-dianisidine as the substrate. Significant levels of peroxidase activity were detected at neutral pH values, as summarized in Table 1. In contrast, the activity dropped to 34% at pH 4.5 and to 3.4% at pH 8.5 as compared to that at pH 6.8 (all measured with H_2O_2 as the reactant and ABTS as the substrate). The changes in the electronic absorption spectrum of the ferric protein upon reaction with hydrogen peroxide or peroxyacetic acid agreed well with formation of the high-valent intermediates known as Compound I and Compound II in the catalytic reaction of plant peroxidases (see below). It should be noted that heme bleaching was only observed when extreme conditions were used, such as very acidic conditions (pH ≤4) or a very large excess (≥1000-fold) of hydrogen peroxide.

Table 1: Comparison of Peroxidase Specific Activities (micromoles per minute per micromole of heme) of NP2, *M. tuberculosis* and *Burkholderia pseudomallei* Catalase-Peroxidases (MtKatG and BpKatG) Measured in This Study under the Same Temperature and Concentration Conditions Using Peroxyacetic Acid (PAA) or Hydrogen Peroxide (H_2O_2) as Reactants and ABTS and *o*-Dianisidine as One-Electron Donors[a]

	ABTS		*o*-dianisidine	
	PAA	H_2O_2	PAA	H_2O_2
NP2 (pH 6.8)	1670 ± 60	43 ± 1	262 ± 4	6 ± 0.15
MtKatG (pH 4.5)	3388 ± 486	1736 ± 25	466 ± 6	1337 ± 47
MtKatG (pH 6.5)	600 ± 80	260 ± 2	nd[b]	nd[b]
BpKatG (pH 4.5)	2750 ± 200	708 ± 20	550 ± 34	725 ± 33
BpKatG (pH 6.5)	250 ± 200	50 ± 2	nd[b]	nd[b]

[a]The reactions were performed in a 1 cm path length cuvette with a final volume of 1 mL, containing 400 μM ABTS or 0.36 mM *o*-dianisidine, with 2.5 mM H_2O_2 or PAA, with addition of appropriately diluted NP2 (1−5 μL of enzyme at a concentration of 9 μM) in 50 mM Tris-maleate at the given pH. [b]Not determined.

Table 1 shows the comparison of the peroxidase specific activity measured for NP2 at pH 6.8 and for the bifunctional peroxidases (KatGs) from *M. tuberculosis* and *B. pseudomallei*. The activities of the KatGs were measured at pH 4.5, the optimum pH for the peroxidase reaction of these bifunctional enzymes (*1*), as well as at pH 6.5 (the optimum pH for the catalase reaction), to have a reference value for low peroxidase activity. Hydrogen peroxide and peroxyacetic acid were used as reactants. ABTS and *o*-dianisidine were used as substrates to test the peroxidase-like activity of NP2. Low levels of specific activity (SA) were measured for both substrates when hydrogen peroxide was used as the reactant, yet the SA value for ABTS was within the low limit shown by BpKatG at pH 6.5. However, when peroxyacetic acid was used as a reactant, the activity levels of NP2 become comparable to those measured for KatGs at their optimal pH (4.5), and considerably higher than the lower limit given by the KatGs at pH 6.5 (Table 1). The comparison of the values obtained from the activity assays on NP2 and KatGs indicates significant activity levels for the nitrophorin. The actual difference in measured values clearly reflects the structural differences of the NP2 heme distal side and/or binding sites for the substrates as compared to typical peroxidases (reviewed in ref *32*). The fact that using peroxyacetic acid as a reactant for NP2 resulted in specific peroxidase activities comparable to those of KatGs (Table 1) suggests that the structural water molecules observed in the heme distal side of NP2 may play important roles. We also determined the kinetic parameters for the peroxidase-like activity of NP2 using ABTS as a substrate. The obtained k_{cat} values were 0.7 s^{-1} with H_2O_2 as the reactant and 29 s^{-1} with PAA. The corresponding K_M values were 1.2 mM (for H_2O_2), 0.58 mM (for PAA), and 0.6 mM (for ABTS) (using PAA). For comparison, the turnover rates (k_{cat}) obtained for MtKatG were 30 s^{-1} for H_2O_2 as the reactant and 56 s^{-1} for PAA, and K_M values of 0.36 mM (for H_2O_2) and 0.07 mM (for ABTS) using PAA as the reactant. It is of note that the kinetic parameters observed for NP2 are within the range of those from other bacterial KatGs (see Table 3 in ref *33*).

The Intermediates of the Peroxidase-like Reaction of NP2 Identified by EPR Spectroscopy. As previously described (*13*), the nearly axial EPR spectrum of NP2, with $g_{\perp}^{eff} \approx 6$ and $g_{||}^{eff} \approx 2$ resonances, is characteristic of heme iron in the ferric (Fe^{III}) high-spin state (Figure 1A, gray trace). The ferric EPR signal, with observed values of 5.94, 5.67, and 1.99 for g_y, g_x, and g_z, respectively, exhibited very weak pH dependence in the pH range from 5 to 9. The dramatic decrease (80%) in the intensity of the ferric signal upon reaction of NP2 at pH 6.0 with a 3-fold excess of peroxyacetic acid (Figure 1A, green trace) indicates the conversion of the high-spin Fe^{III} state to a higher-valence intermediate. The new EPR signal, with observed values of 4.03, 3.80, and 2.00 for g_y^{eff}, g_x^{eff}, and g_z^{eff}, respectively (Figure 1A, green trace), which appeared concomitantly with the disappearance of the ferric signal, agrees well with the EPR spectrum previously reported for $a_{2u}(\pi)$ porphyrin radical complexes (*24*−*27*). The latter were assigned to the $S = {}^3/_2$ signal of an $[Fe^{IV}{=}O\ Por^{\bullet}]^+$ species with strong ferromagnetic coupling interaction between the porphyrin π-radical and the ferryl iron (*24*−*27*). It should be noted that the EPR signal of an organic radical (< 10%) is superimposed on the g_z component of the $[Fe^{IV}{=}O\ Por^{\bullet}]^+$ species, which would otherwise be expected to be a negative feature at $g = 1.99$ (see Figure 5 of ref *27*). The contribution of this narrow organic radical signal modestly increased when a larger excess of peroxyacetic acid was used.

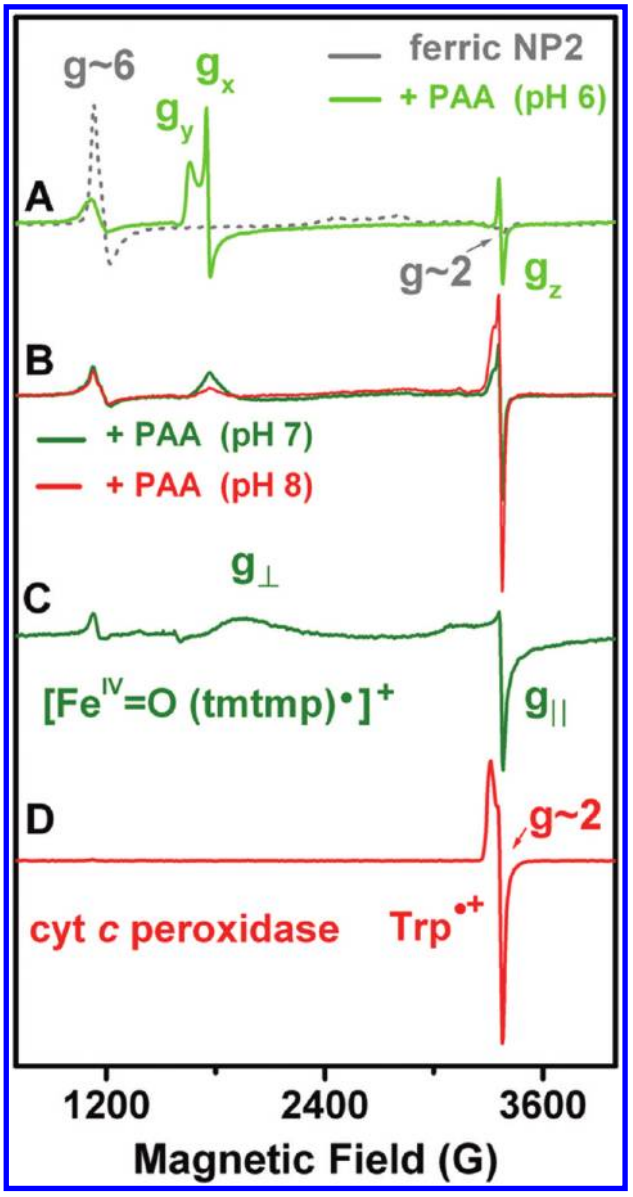

FIGURE 1: EPR spectra (9 GHz) of the intermediates formed by the reaction of nitrophorin 2 (NP2) with a 3-fold excess of peroxyacetic acid (PAA) at pH 6 (A, green trace), pH 7 (B, dark green trace), and pH 8 (B, red trace). The ferric signal of NP2 prior to the reaction mixture is also shown (A, gray dotted trace). For comparison to spectrum B, the axial signal of the $a_{1u}(\pi)$ porphyrin radical species (C, green trace) obtained from the oxidation of the $[Fe^{III}(tmtmp)]$ triflate model complex and the signal of the exchange-coupled $Trp^{\bullet+}$ of cytochrome *c* peroxidase were measured under the same experimental conditions. Spectra were recorded at 4 K with a 4 G modulation amplitude, a 1 mW microwave power, and a 100 kHz modulation frequency. The final concentrations in the samples were 0.25 mM NP2 and 0.75 mM PAA for spectra A and B and 0.25 mM CcP and 0.25 mM H_2O_2 for spectrum D.

At pH 7, the EPR spectrum that results from the reaction of NP2 with peroxyacetic acid (Figure 1B, dark green trace) clearly differs from the spectrum obtained at pH 6 (Figure 1A, green trace). The contribution of two different EPR signals could be discerned by the variation of their relative intensities as a function of pH (Figure 1B, dark green and red traces). Specifically, the change from neutral to basic pH induced a decrease in the $g = 3.8$ resonance and a concomitant increase in intensity of the 250 G broad signal centered at $g \approx 2$ in the EPR spectrum. The $g = 3.8$ resonance is consistent with the $g_{\perp}^{eff}$ of

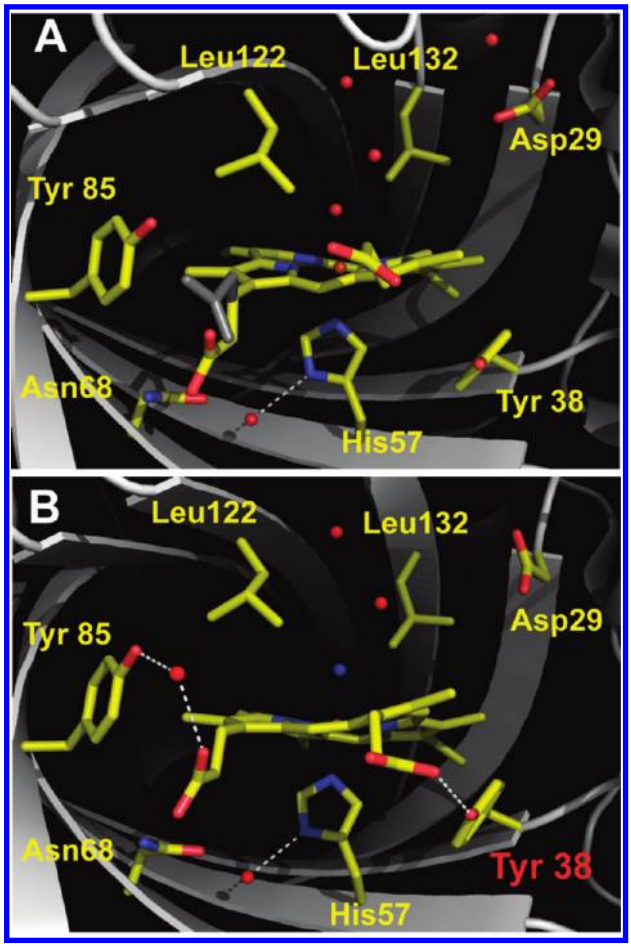

FIGURE 2: Crystallographic structure of nitrophorin 2 at pH 6.5 (A) and pH 7.7 (B), highlighting the environment of the heme active site. An NH_3 molecule (blue, B), supplied by the $(NH_4)_2HPO_4$ crystallization buffer at pH 7.7, or a water molecule at pH 6.5 constitutes the sixth ligand. Tyr38 is within H-bonding distance of the 7-propionate only at the higher pH. The two possible conformations adopted, with equal preference, by the 7-propionate at pH 6.5 are also shown in panel A. This figure was prepared using the coordinates deposited in the Protein Data Bank (entry 1EUO for pH 7.7 and entry 2A3F for pH 6.5).

the axial signal of an $[Fe^{IV}{=}O\ Por^{\bullet}]^+$ species ($g_{\perp}^{eff} = 3.80$, and $g_{\parallel}^{eff} = 1.99$) expected for an $a_{1u}(\pi)$ radical, as previously reported for ferryl porpholactone radical complexes (*34*) and iron porphyrins that are highly nonplanar, but not ruffled (*27*, *28*). The EPR spectrum of the Compound I π-cation radical obtained upon oxidation of the $[Fe^{III}(tmtmp)]$ triflate model complex, recorded under the same conditions that were used for NP2, is shown for comparison (Figure 1C). The latter was assigned to an $S = {}^3/_2$ species with weak ferromagnetic coupling (*28*). Hence, the changes from acidic (Figure 1A, green trace) to neutral (Figure 1B, dark green trace) pH in NP2 directly correlated with the change from strong to weak ferromagnetic interactions between the ferryl iron and the radical delocalized over the porphyrin moiety of the $[Fe^{IV}{=}O\ Por^{\bullet}]^+$ species. The latter, known as Compound I, is the first committed intermediate in the catalytic cycle of peroxidases (reviewed in ref *32*).

The 250 G broad signal, centered at $g \approx 2$, that contributed to the EPR spectra of the NP2 intermediate obtained at pH 7 and 8 (Figure 1B) was the predominant signal at basic pH. The overall width (250 G) and the distinct temperature dependence of this signal were consistent with an organic radical in a magnetic interaction with the ferryl heme iron, as in the case of the

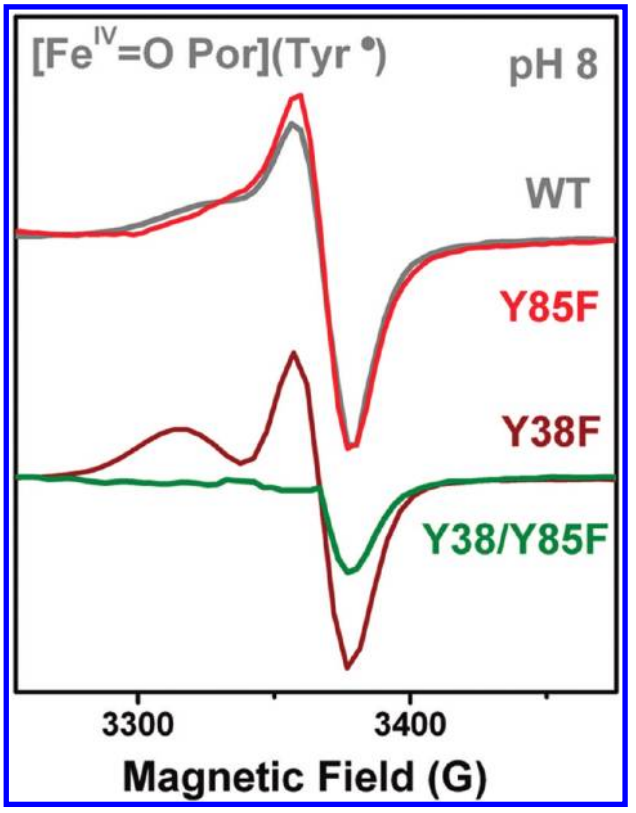

FIGURE 3: EPR spectra (9 GHz) of the $[Fe^{IV}{=}O\ Por](Tyr^{\bullet})$ intermediate formed upon reaction of wild-type NP2 (gray trace) and Tyr variants with peroxyacetic acid. Both NP2 and peroxyacetic acid were at pH 8. Experimental conditions and sample concentrations were as described in the legend of Figure 1.

$[Fe^{IV}{=}O\ Por](Trp191^{\bullet})^+$ species in cytochrome *c* peroxidase (Figure 1D), recorded under the same conditions that were used for NP2. As was previously shown for cytochrome *c* peroxidase (*35*), modification of the intrinsic *g* values of a protein-based radical due to the contribution of the exchange coupling interaction impedes direct determination of the chemical nature of the radical by means of the EPR spectrum, even with the advantageous resolution of higher frequencies and/or higher fields (*35*). Our alternative approach for identifying the protein-based radical site in NP2 was to design mutations based on inspection of the crystal structure of NP2 [Protein Data Bank (PDB) entry 1EUO at pH 7.7 (*11*)] and consider the physical constraints inferred from the EPR studies. Accordingly, Tyr38 and Tyr85 were identified as the most suitable candidates for the exchange-coupled radical, because of their proximity and/or H-bonding interaction with the heme iron (Figure 2). Thus, three Tyr mutants (Y38F, Y85F, and the Y38F/Y85F double mutant) were designed, expressed, and purified so that their intermediates could be characterized by EPR spectroscopy.

Upon reaction of the single and double mutants of NP2 at pH 8 with peroxyacetic acid, only minor changes in shape of the $g_{\perp}^{eff}$ component of the $[Fe^{IV}{=}O\ Por^{\bullet}]^+$ species were observed, as compared to the wild-type case (resonance at $g = 3.8$ in Figure 1B). For the sake of clarity, only the enlargement of the $g \approx 2$ region of the EPR spectra of the intermediates is shown in Figure 3. The Y38F and Y85F single mutants of NP2 both showed the broad and temperature-dependent signal (250 G wide) of the exchange-coupled protein-based radical, yet closer inspection of the EPR spectrum revealed an important difference. The Y85F signal (Figure 3, red trace) was very similar to that of the wild-type

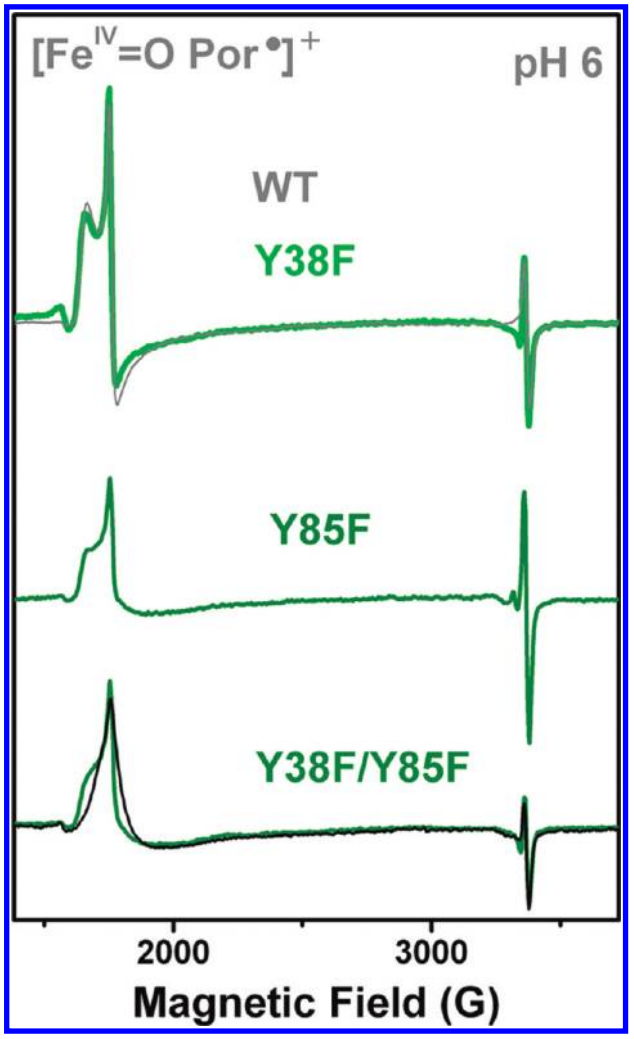

FIGURE 4: EPR spectra (9 GHz) of the [Fe^{IV}=O Por$^{\bullet}$]$^{+}$ intermediate formed upon reaction of wild-type NP2 (gray trace) and Tyr variants with peroxyacetic acid. Both NP2 and peroxyacetic acid were at pH 6. The spectrum obtained for the double mutant Y38F/Y85F at pH 8 (bottom, black trace) is also shown. Experimental conditions and sample concentrations were as described in the legend of Figure 1.

protein (Figure 3, gray trace). In contrast, a noticeable change in the shape of the broad signal was observed in the case of the Y38F sample (Figure 3, dark red trace), which indicates a modification of the magnetic interaction between the tyrosyl radical and the heme iron, only in the case of the Y38F mutation. Moreover, the EPR spectrum of the double mutant Y38F/Y85F at pH 8 showed no protein-based radical signal (Figure 3, green trace); only the [Fe^{IV}=O Por$^{\bullet}$]$^{+}$ species was formed at both acid and basic pH values (Figure 4). The effect on the shape of the EPR spectrum induced by the Y38F mutation could be explained by either changes in the relative position of the Tyr radical site and the heme propionate or the formation of the radical on a different site. Hence, the Y38F/Y85F double mutant, in which both candidates for the radical site were removed, was crucial for rationalizing the effect of the single mutations.

Taken together, these findings indicate that Tyr38 is the primary site for the formation of the protein-based radical, because the radical spectrum of the Y85F variant was the same as in the wild-type protein. Nonetheless, when this site was suppressed (Y38F mutant), the radical formed on Tyr85. The difference in the shape of the 250 G-wide signal observed for the Y38F sample, as compared to those of the wild type and Y85F (Figure 3), strongly suggests mild, but measurable, differences in the exchange-coupled ferromagnetic interaction of the radical and the heme iron. The differences in H-bonding interactions of Tyr38 and Tyr85 with the propionates (see Figure 2) could account for such an effect. The fact that only the [Fe^{IV}=O Por$^{\bullet}$]$^{+}$ species was formed in the double Tyr mutant (Figure 4) clearly indicated that Tyr38 and Tyr85 are the only sites for the [Fe^{IV}=O Por](Tyr$^{\bullet}$) intermediate, with the Tyr85 radical being formed only if the naturally occurring site Tyr38 was removed.

The reaction of NP2 with hydrogen peroxide was also monitored by EPR spectroscopy. As in the case of peroxyacetic acid, a dramatic decrease in intensity of the ferric EPR signal when the protein was mixed with either a 40- or 400-fold excess of H_2O_2 indicated the conversion to an EPR silent and higher-valence intermediate. Only a minor contribution (< 15% in spin concentration) of a narrow radical at $g = 2$ was observed when using a larger excess of H_2O_2 at pH 8.0 (Figure S2 of the Supporting Information). The EPR-silent species can confidently be assigned to the [Fe^{IV}=O Por] intermediate that is known as Compound II in peroxidases and indicates a fast conversion of the [Fe^{IV}=O Por$^{\bullet}$]$^{+}$ species to Compound II in the NP2 reaction with H_2O_2. The electronic absorption spectra obtained by the stopped-flow experiments crucially confirmed this assignment (see Figure 6).

Kinetic Studies by Stopped-Flow Electronic Absorption Spectrometry. The reaction of NP2 with either peroxyacetic acid or hydrogen peroxide was monitored by using conventional dual-syringe mixing and a diode array detector attached to the stopped-flow instrument. The measurements taken at 5 and 20 °C showed the same spectral changes for the reaction. The choice of 5 °C as a measuring temperature allowed us to better characterize the reaction, because the rate of conversion between intermediates slowed considerably as a function of temperature, as previously shown in the case of lactoperoxidase (*36*). Such a choice also allowed us to more accurately assess the chemical nature of the intermediates, by combining the information obtained from the electronic absorption experiments and EPR spectroscopy.

It is worth mentioning that the [Fe^{IV}=O Por$^{\bullet}$]$^{+}$ and [Fe^{IV}=O Por] species, known as Compound I and Compound II, respectively, in catalases and peroxidases, exhibit quite distinct bands in their electronic absorption spectra, because the delocalization of the radical over the porphyrin affects the electronic state and coupling. In contrast, the absorption spectrum of an [Fe^{IV}=O Por](Tyr$^{\bullet}$) species is indistinguishable from an [Fe^{IV}=O Por] (Compound II) species, because the absorption band of the Tyr$^{\bullet}$ is masked by those of the heme, while the EPR spectrum of the Tyr$^{\bullet}$ makes clear the difference between the [Fe^{IV}=O Por](Tyr$^{\bullet}$) species and the EPR-silent [Fe^{IV}=O Por] species, which has been previously shown (*37*). Accordingly, it is necessary to combine the information obtained from the EPR spectra for the electronic structure of the species with that of the rapid-scan absorption spectra for the kinetics of the reactive intermediates to facilitate the analysis of the catalytic intermediates in NP2 and their reactivity with substrates. It is of note that the much higher concentrations of protein, oxidants, and/or substrates used in the EPR experiments compared to those of the kinetic studies imply that the transition rates between intermediates will be different.

Panels A and B of Figure 5 show changes in the electronic absorption spectrum of NP2 at pH 6.0 and 8.0, respectively, upon

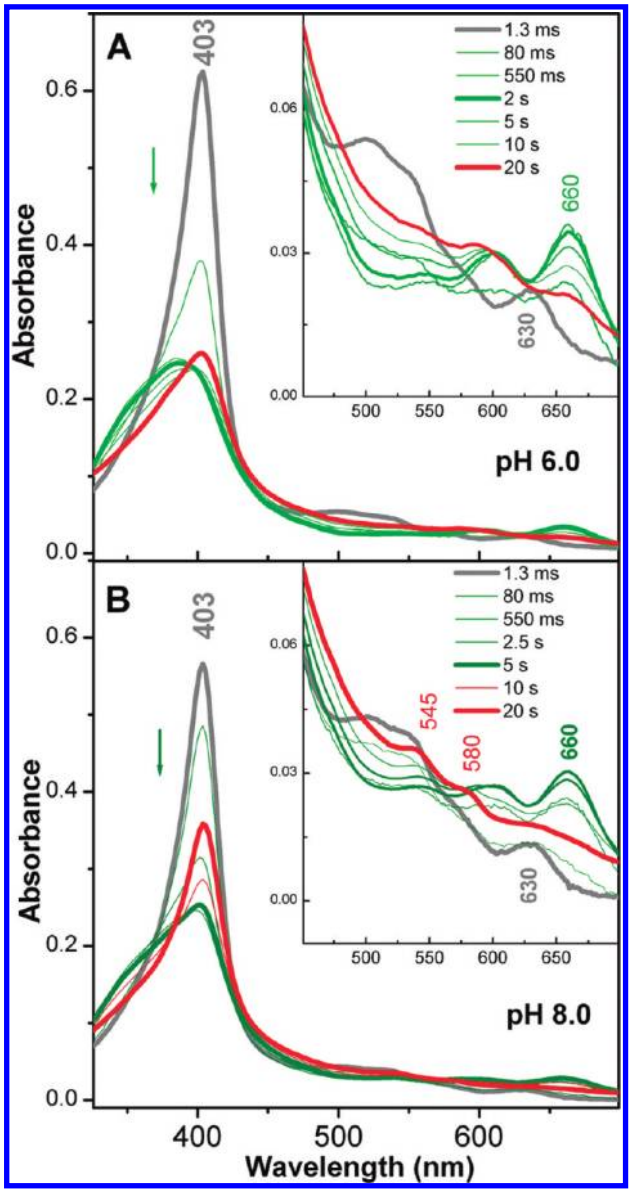

FIGURE 5: Rapid-scan electronic absorption spectra of the reaction of NP2 with peroxyacetic acid. Protein and reactant (final) concentrations were 5 and 10 μM, respectively. The samples and mixing chamber were kept at 5 °C, and the reaction was monitored up to 20 s. The experiments were conducted at pH 6 (A) and pH 8 (B). Selected representative spectra are shown. The spectrum of the native (ferric) enzyme is colored gray, that of the $[Fe^{IV}{=}O\ Por^{\bullet}]^{+}$ species green, and that of the one-electron-reduced $[Fe^{IV}{=}O\ Por]$ (Compound II) intermediate red.

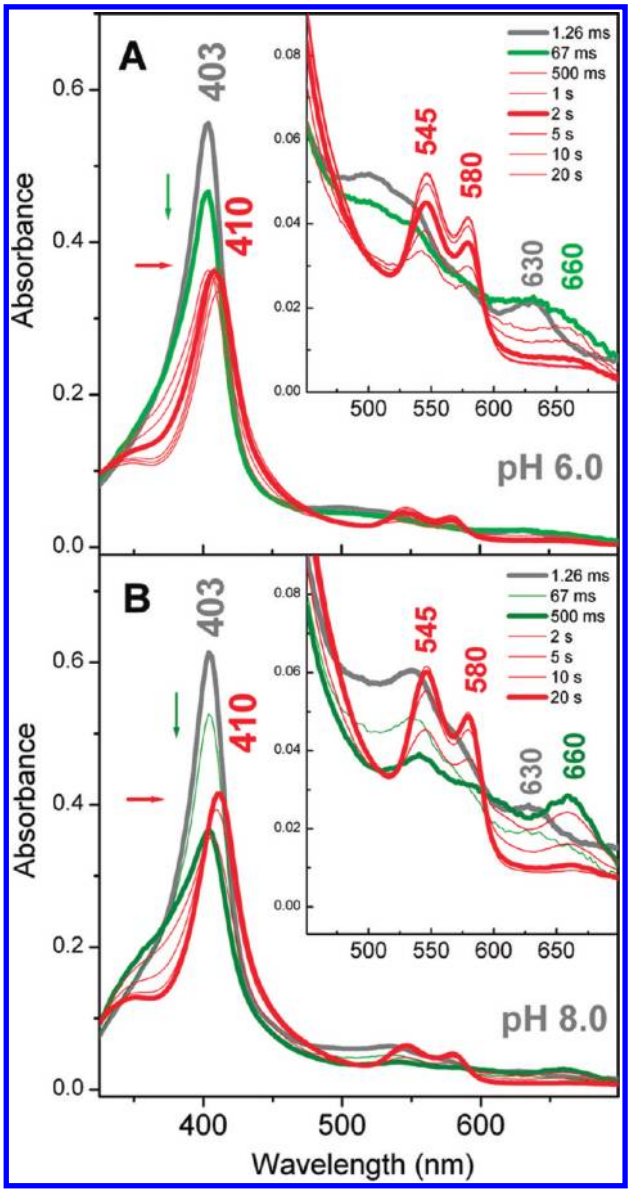

FIGURE 6: Rapid-scan electronic absorption spectra of the reaction of NP2 with hydrogen peroxide. Protein and reactant (final) concentrations were 5 μM and 2 mM, respectively. The samples and mixing chamber were kept at 5 °C, and the reaction was monitored up to 20 s. The experiments were conducted at pH 6 (A) and pH 8 (B). Selected representative spectra are shown. The spectrum of the native (ferric) enzyme is colored gray, that of the $[Fe^{IV}{=}O\ Por^{\bullet}]^{+}$ species green, and that of the one-electron-reduced $[Fe^{IV}{=}O\ Por]$ (Compound II) intermediate red.

reaction with a 2-fold excess of peroxyacetic acid and as a function of time, on the millisecond time scale, and up to 20 s. The electronic absorption spectrum of the protein before reaction with peroxyacetic acid shows the characteristic bands of ferric high-spin heme peroxidases, with the Soret band at 403 nm and the charge-transfer band at 630 nm at both pH values (Figure 5A, B, gray traces). The new species showed clear hypochromicity of the Soret band and a shift of the charge-transfer band to 660 nm and was partially formed within 80 ms at pH 6 (Figure 5A, green traces). Full conversion was observed within 550 ms, and the new species remained stable for several seconds (thick green trace). The final spectrum (Figure 5A, red trace) showed a narrowing of the Soret band and two ill-defined bands at ~545 and ~580 nm. Spectral analysis of the rapid-scan electronic absorption spectra using a two-step model (A → B → C) yielded an observed rate constants k_1 of 11 s^{-1} for the transition of the ferric protein (gray trace) to species B (green trace) and a final species C (red trace) being formed very slowly (k_2 = 0.09 s^{-1}). The spectral features of species B (Figure 5A, thick green trace) were consistent with those of the $[Fe^{IV}{=}O\ Por^{\bullet}]^{+}$ intermediate, in total agreement with the EPR spectrum (see the green trace in Figure 2A).

When the reaction of NP2 and peroxyacetic acid at pH 8 (Figure 5B) was monitored, the observed spectral changes were qualitatively comparable to those described for the pH 6 case, although a clearly slower formation of species B (Figure 5B, dark green traces) and a faster conversion to species C (Figure 5B, thick red trace) were observed. Also, the spectrum of the final

Table 2: Calculated Rate Constants (k_{obs} in inverse seconds) for the Reaction of Nitrophorin 2 with Peroxyacetic Acid (PAA) and Hydrogen Peroxide as a Function of pH[a]

	pH 6		pH 8	
	PAA	H_2O_2	PAA	H_2O_2
k_1	11.0	9.67	4.54	4.29
k_1'		20.06	0.88	8.41
k_2	0.09	0.67	0.14	0.27

[a]Models accounting for two steps (ferric → Compound I → Compound II, with k_1 and k_2, respectively) and three steps (ferric → Compound I → [Fe^{IV}=O Por](Tyr•) → Compound II, with k_1, k_1', and k_2, respectively) were used (see Results). Measurements were taken at 5 °C. The reactant final concentration was 10 μM for PAA and 2 mM for H_2O_2, with a final protein concentration of 5 μM in both cases.

species C showed the well-defined features characteristic of an [Fe^{IV}=O Por] (Compound II) species (the Soret band shifted to 410 nm, and the α and β bands at 580 and 545 nm, respectively). Even though the rapid-scan electronic absorption spectrum of the reaction of NP2 at pH 8 could be analyzed in terms of a two-step model (ferric → [Fe^{IV}=O Por•]$^+$ → [Fe^{IV}=O Por]) as in the case of pH 6, a three-step model (A → B → B′ → C with corresponding transition rates k_1, k_1', and k_2, respectively) would take into account the formation of the tyrosyl radical intermediate (species B′) obtained from the EPR spectroscopic characterization (Figure 2B). Hence, the calculated rate constants were as follows: $k_1 = 4.54\ s^{-1}$, $k_1' = 0.88\ s^{-1}$, and $k_2 = 0.14\ s^{-1}$ (see Table 2). The observed transition rate of 4.54 s^{-1} for the ferric protein to [Fe^{IV}=O Por•]$^+$ conversion reflected the slower formation of the [Fe^{IV}=O Por•]$^+$ intermediate at pH 8 versus that at pH 6 (k_1 = 11 s^{-1}). The spectrum of species B′ (with a transition rate k_1' of 0.88 s^{-1}) showed contributions of the characteristic bands of both [Fe^{IV}=O Por•]$^+$ (species B) and a Compound II-like species, in agreement with the EPR spectrum at pH ≥7 (Figure 1B). As previously shown, the electronic absorption spectrum of an [Fe^{IV}=O Por](Tyr•) species is indistinguishable from those of the [Fe^{IV}=O Por] (Compound II) species (*36*); thus, the spectral analysis alone would fail to identify the intermediate. Hence, the EPR characterization was crucial for assessing the formation of a protein-based radical intermediate at pH 8.

When hydrogen peroxide was used as the reactant, the [Fe^{IV}=O Por•]$^+$ intermediate was shorter-lived at both pH values and readily converted to the [Fe^{IV}=O Por] (Compound II) intermediate (Figure 6A,B). When the reaction was performed at pH 6.0, the spectral features of the [Fe^{IV}=O Por] (Compound II) species, with the characteristic shift of the Soret band to 410 nm and the α and β bands at 580 and 545 nm, respectively (Figure 6A, thick red trace), were already contributing to the spectrum of the very short-lived [Fe^{IV}=O Por•]$^+$ species (Figure 6A, green trace). Consistently, the EPR results showed the conversion of the ferric signal to an EPR-silent species in the time scale of manual mixing of NP2 and hydrogen peroxide (2 s). At pH 8.0 (Figure 6B), the [Fe^{IV}=O Por•]$^+$ species was longer-lived (Figure 6B, thick green trace) yet converted to the Compound II species in less than 1 s. The calculated rate constants are listed in Table 2. A similarly rapid, spontaneous decay of the [Fe^{IV}=O Por•]$^+$ intermediate to the Compound II species was previously reported for the reaction of lactoperoxidase with hydrogen peroxide (*36*), as well as lignin and ascorbate peroxidases (*38*).

It should be noted that both peroxyacetic acid and hydrogen peroxide exhibited the same pH-dependent effect on the formation of the [Fe^{IV}=O Por•]$^+$ and [Fe^{IV}=O Por] (Compound II) species, which was a slower formation of the [Fe^{IV}=O Por•]$^+$ intermediate followed by a faster conversion to the [Fe^{IV}=O Por] (Compound II) species at pH 8 (see Table 2). It is of note that the observed rate constants listed in Table 2 correspond to pseudo-first-order rate constants and that the concentration of H_2O_2 (2 mM) used in these experiments was much higher than that of PAA (10 μM). Hence, because k_1 is directly proportional to the reactant concentration, the bimolecular rate constants for the formation of the [Fe^{IV}=O Por•]$^+$ species at pH 6 would be $1.7 \times 10^5\ M^{-1}\ s^{-1}$ for PAA and $0.7 \times 10^3\ M^{-1}\ s^{-1}$ for H_2O_2. The effect of pH on the rates of Compound I and Compound II formation has been shown for several peroxidases, such as peanut and horseradish peroxidases (see ref *32* and references cited therein).

Peroxidase-like Reaction of NP2 with Norepinephrine and Other Substrates. After we had demonstrated that NP2 has significant levels of peroxidase-like activity when ABTS and *o*-dianisidine are used as substrates (see Table 1), and that NP2 formed both the [Fe^{IV}=O Por•]$^+$ and [Fe^{IV}=O Por](Tyr38•) intermediates in a peroxidase-like pathway, we used stopped-flow electronic absorption spectrophotometry to characterize the putative enzymatic reaction with benzohydroxamic acid, norepinephrine, and histamine. Norepinephrine and histamine are relevant for addressing the question of the putative biological role of the peroxidase-like activity in nitrophorins and its relationship to the main functions of the protein, i.e., NO and histamine binding. BHA, a well-characterized aromatic substrate for peroxidases (see, for example, ref *36*), was chosen for the comparisons with norepinephrine and histamine. The choice of peroxyacetic acid as a reactant was based on the fact that both peroxyacetic acid and hydrogen peroxide showed the same effect of pH on the formation of the [Fe^{IV}=O Por•]$^+$ and the ferryl species, but the turnover was slower with peroxyacetic acid. Accordingly, the latter was the reactant of choice for monitoring of the peroxidase-like reaction of the intermediates with the three different molecules mentioned above.

The peroxidase-like reaction of BHA, norepinephrine, and histamine with NP2 was monitored at pH 6 and 8, by using the sequential mixing technique in combination with the diode array detector. In all experiments, the [Fe^{IV}=O Por•]$^+$ intermediate was preformed by mixing the protein with a 2-fold excess of peroxyacetic acid in the aging loop for 500 ms (at pH 6) or 1.85 s (at pH 8), prior to the reaction with a 5-fold excess of each substrate. Hence, the final concentrations (after the two mixing steps) for NP2, PAA, and substrate were 15, 30, and 75 μM, respectively. This approach was used to specifically monitor the putative one-electron reaction of the [Fe^{IV}=O Por•]$^+$ intermediate with each of the three molecules. Another reason for using this approach was that the direct mixing of the ferric high-spin protein with histamine or norepinephrine led to formation of ferric low-spin complexes, with the characteristic shift of the Soret band to 408−410 nm and a broad α and β band in the 525−600 nm spectral region (see Figure S1A of the Supporting Information). Such a spectrum was very similar to those of the previously reported NP−histamine complexes (*16*). The corresponding EPR spectra confirmed the formation of the ferric low-spin complexes of NP2 with histamine and norepinephrine at low temperatures (see Figures S4B and S5 of the Supporting Information). The NMR spectra of the norepinephrine complex at room temperature were also those of a low-spin heme complex in which the ligand is bound to iron via the amino group (see Figures S8−S12 of

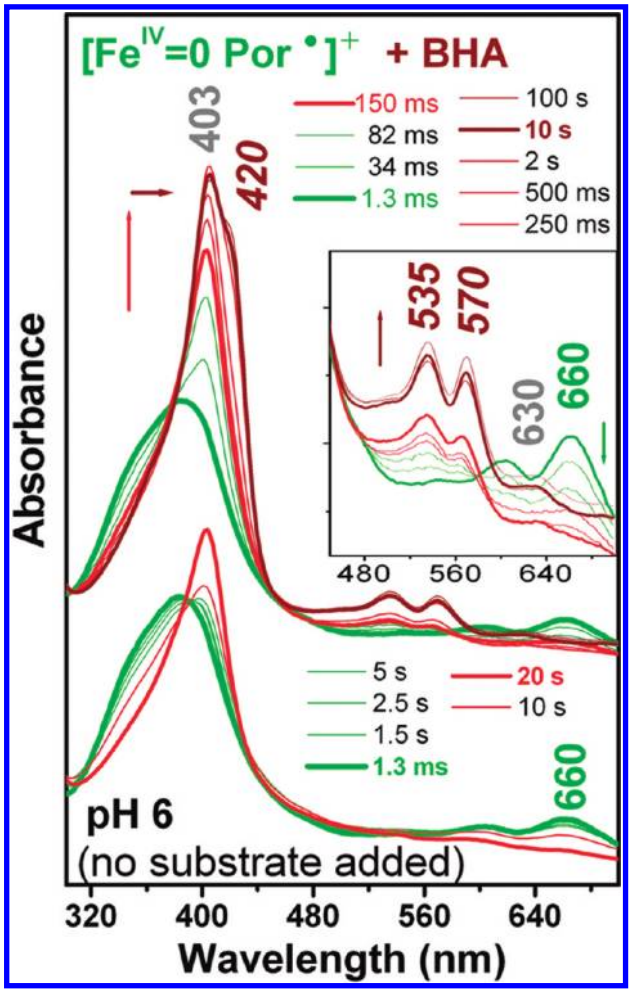

FIGURE 7: Rapid-scan electronic absorption spectra of the peroxidase-like reaction of the $[Fe^{IV}=O\ Por^{\bullet}]^{+}$ intermediate (pH 6) with benzohydroxamic acid (BHA) as the substrate. The control sample (bottom) corresponds to the use of buffer instead of substrate. Sequential mixing, combined with diode array detection, was used to monitor the reaction at 5 °C of the preformed $[Fe^{IV}=O\ Por^{\bullet}]^{+}$ species with BHA. Only representative spectra are shown, and the 1.3 ms spectrum represents the first recorded spectrum upon reaction with BHA. Final concentrations were 5, 10, and 25 μM for NP2, PAA, and BHA, respectively. The experimental conditions are further described in Materials and Methods.

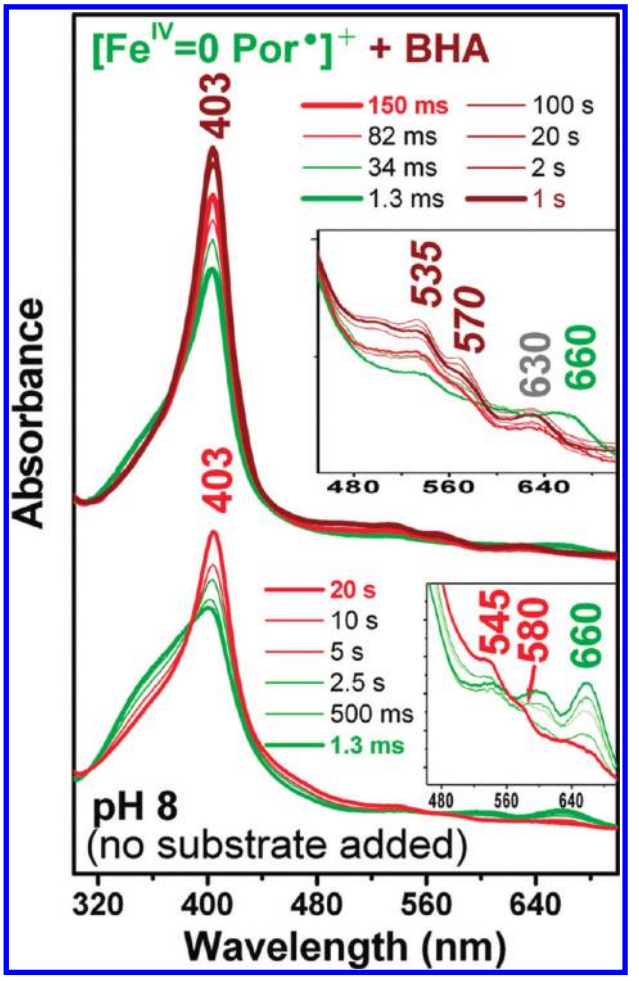

FIGURE 8: Rapid-scan electronic absorption spectra of the peroxidase-like reaction of the $[Fe^{IV}=O\ Por^{\bullet}]^{+}$ intermediate (pH 8) with benzohydroxamic acid (BHA) as the substrate. The $[Fe^{IV}=O\ Por^{\bullet}]^{+}$ intermediate (green trace) was preformed with peroxyacetic acid and a mixing time of 1.5 ms at 5 °C. Only representative spectra are shown. Final samples concentrations were 5, 10, and 25 μM for NP2, peroxyacetic acid, and BHA, respectively. The experimental conditions are further described in Materials and Methods.

the Supporting Information); the NMR spectrum of the histamine complex at room temperature, in which histamine is bound to iron through the imidazole group, has been published previously (*39*). In contrast, no modification of the ferric high-spin spectrum of NP2 was observed when a 5-fold excess of BHA was added (Figure S4 of the Supporting Information); NMR spectra at ambient temperature also showed no modification, as discussed in the Supporting Information. Accordingly, once the low-spin complexes of NP2 with norepinephrine or histamine were formed, the absence of further reaction with peroxyacetic acid or hydrogen peroxide was indicative of an inhibitory effect of norepinephrine and histamine on the peroxidase-like activity of the resting (ferric) NP2.

Benzohydroxamic Acid. The rapid-scan optical spectra of the reaction of the preformed $[Fe^{IV}=O\ Por^{\bullet}]^{+}$ intermediate of NP2 (see above) with BHA are shown in Figure 7 (pH 6) and Figure 8 (pH 8). At pH 6, the reaction of the $[Fe^{IV}=O\ Por^{\bullet}]^{+}$ intermediate with BHA was shown by the spectral changes observed within 150 ms (Figure 7 top, thick red trace), as compared to the control experiment (no BHA added). In the latter, the $[Fe^{IV}=O\ Por^{\bullet}]^{+}$ intermediate was stable for several seconds (Figure 7, bottom, green traces). Interestingly, and at variance with the case of peroxidases (see, for example, Figure 4 in ref *36*), the spectral features characteristic of the $[Fe^{IV}=O\ Por]$ (Compound II) species (Soret band shifted to 410 nm and α and β bands at 580 and 545 nm, respectively), which were expected as a result of the one-electron oxidation of BHA by the $[Fe^{IV}=O\ Por^{\bullet}]^{+}$ intermediate, were not detected (Figure 7, top). Instead, the new spectra observed concomitantly with the disappearance of the $[Fe^{IV}=O\ Por^{\bullet}]^{+}$ species showed the Soret band at 403 nm and the charge-transfer band at 630 nm (Figure 7 top, red traces), plus the contribution of another species with new bands at 420, 535, and 570 nm (Figure 7A, dark red traces), a spectrum strongly reminiscent of that of the NP2−NO complex (*15*). These findings could be rationalized in terms of a fast one-electron reaction of the $[Fe^{IV}=O\ Por]$ (Compound II) species with BHA, which brought the protein back to the initial ferric high-spin state. The latter converted slowly to a ferric low-spin type of the optical spectrum. Addition of BHA to the ferric protein in the absence of peroxyacetic acid did not result in the formation of the low-spin complex. Thus, the peroxidase-like

Table 3: Calculated Rate Constants (k_{obs} in inverse seconds) for the Peroxidase-like Reaction of the Preformed $[Fe^{IV}=Por^{\bullet}]^{+}$ Intermediate (species A) of NP2 with Benzohydroxamic Acid (BHA), Histamine, and Norepinephrine (Nor) as Substrates[a]

	Buffer	BHA	Histamine	Norepinephrine
pH 6				
k_1	0.04	8.5	0.2	270
k_2		1.0		
	A→ Fe^{IV}=O	A→Fe^{III} (high spin) →Fe^{III}-low spin complex	A→Fe^{IV}=O	A→Fe^{III}
pH 8				
k_1	0.11	14.6 [a]	0.6	227
k_2		5.1 [a]		1.6
	A→ Fe^{IV}=O	A→Fe^{III} (high spin) →Fe^{III}-low spin complex	A →Fe^{III}-Hm	A→Fe^{III} →Fe^{III}-Nor

[a]Measurements were performed at 5 °C. Models that account for one step (A→B,with k_1) and two steps (A→B→C, with k_1 and k_2, respectively) were used. Species B and C have different electronic structures depending on the substrate. The [Fe^{IV}=O Por] intermediate resulted from the reaction of the $[Fe^{IV}=O\ Por^{\bullet}]^{+}$ species with each substrate. The further reaction of the [Fe^{IV}=O Por] intermediate with each substrate brought the protein back to the ferric state (see the text). Thus, k_1 represents both reactions, except in the case of histamine at pH 6. The final concentrations (after the two mixing steps) for NP2, PAA, and substrates were 5, 10, and 25 μM, respectively. [b]To account for the already partial reaction of the $[Fe^{IV}=O\ Por^{\bullet}]^{+}$ species with BHA at pH 8 within the first 1.3 ms (Figure 6A, green trace), the pure $[Fe^{IV}=O\ Por^{\bullet}]^{+}$ spectrum from the control experiment (Figure 6B, green trace) was used as the first spectrum for the SVD analysis of the data.

reaction of NP2 with BHA may have resulted in the oxidation of the NHOH group to NO or HNO (*40*−*42*), which could then form a low-spin NO or HNO complex with the ferric heme.

At pH 8, the first spectrum, recorded 1.3 ms after the reaction of the NP2 intermediate with BHA (Figure 8, top, green trace), was equivalent to the transitional spectrum of the spontaneous decay of the $[Fe^{IV}=O\ Por^{\bullet}]^{+}$ intermediate observed at ∼2.5 s in the control experiment [in which buffer was used instead of BHA (Figure 8, bottom)]. Accordingly, the reaction of the $[Fe^{IV}=O\ Por^{\bullet}]^{+}$ intermediate with BHA was substantially faster at pH 8 than at pH 6 (see Table 3), yet the bands of the species observed upon reaction with BHA agreed well with those of the ferric high-spin species (403 and 630 nm), with a relatively smaller contribution of the low-spin complex (Figure 8 top, dark red trace), as compared to the pH 6 case. If one considers that in the control experiment, the [Fe^{IV}=O Por] (Compound II) intermediate formed very slowly by spontaneous decay of the $[Fe^{IV}=O\ Por^{\bullet}]^{+}$ species (Figure 8, bottom, red traces), the results observed upon reaction with BHA were indicative of a fast formation and subsequent reaction (within ∼80 ms) of the [Fe^{IV}=O Por] (Compound II) intermediate with BHA at pH 8.

Histamine. The rapid-scan electronic absorption spectra of the reaction of the preformed $[Fe^{IV}=O\ Por^{\bullet}]^{+}$ intermediate of NP2 with histamine are shown in Figure 9. At pH 6, the conversion of the $[Fe^{IV}=O\ Por^{\bullet}]^{+}$ intermediate (Figure 9A, green traces) to the [Fe^{IV}=O Por] (Compound II) species with characteristic bands at 410, 545, and 580 nm (Figure 9A, red traces) was indicative of a typical, yet extremely slow, peroxidase-like one-electron reaction of NP2 with histamine. It is of note that the rates (see Table 3) are comparable to those of the spontaneous decay observed in the absence of substrate (Figure 7, control). At pH 8, the [Fe^{IV}=O Por] (Compound II) species that results from the peroxidase-like reaction of NP2 with histamine was not detected. Instead, the resulting species was a low-spin ferric complex of NP2 and histamine [shift of the Soret band to 410 nm and a broad α and β band in the 525−600 nm spectral region (Figure 9B, dark red trace)]. This result can be rationalized by the fact that the reduction of the [Fe^{IV}=O Por] (Compound II) species by histamine is much faster than the reduction of the $[Fe^{IV}=O\ Por^{\bullet}]^{+}$ intermediate, such that no detectable Compound II builds up during the reaction. Hence, the protein cycled back to the ferric oxidation state with histamine bound, and both the reaction and binding were favored by the basic pH. The optical and EPR spectra of NP1−NP4 in the presence of histamine have been reported in detail (*43*, *44*).

Norepinephrine. The rapid-scan electronic absorption spectra showed a much faster reaction of NP2 with norepinephrine (Figure 9C,D and Table 3). The full conversion of the $[Fe^{IV}=O\ Por^{\bullet}]^{+}$ intermediate back to the ferric state was observed within 12 ms at pH 6 or 6 ms at pH 8. The [Fe^{IV}=O Por] (Compound II) species was not detected, as in the case of the histamine reaction at pH 8 or the BHA reaction at both pH values, and hence is also interpreted in terms of a much faster reduction of the [Fe^{IV}=O Por] (Compound II) species by norepinephrine than the reduction of $[Fe^{IV}=O\ Por^{\bullet}]^{+}$ by the same substrate. Provided that the reaction of norepinephrine with Compound II was sufficiently fast, the intermediate would never build up to detectable levels. Interestingly, the final oxidation state that results from the reaction of NP2 at pH 6 with norepinephrine was ferric high-spin (Figure 9C, gray trace), which was formed within 12 ms. At pH 8, the fast peroxidase-like reaction resulted in the spectrum of the high-spin ferric protein (Figure 9D, thick gray trace), which was formed within 6 ms, but a subsequent and slow conversion (within 1 s) to the ferric low-spin spectrum (Figure 9D, thick dark-red trace) was also observed. This low-spin species was shown to have the same EPR spectrum (see Figure S5 of the Supporting Information) as that obtained by direct addition of either norepinephrine (see Figure S4 of the Supporting Information) or *n*-butylamine to NP2, and thus likely represents the binding of the amino group of

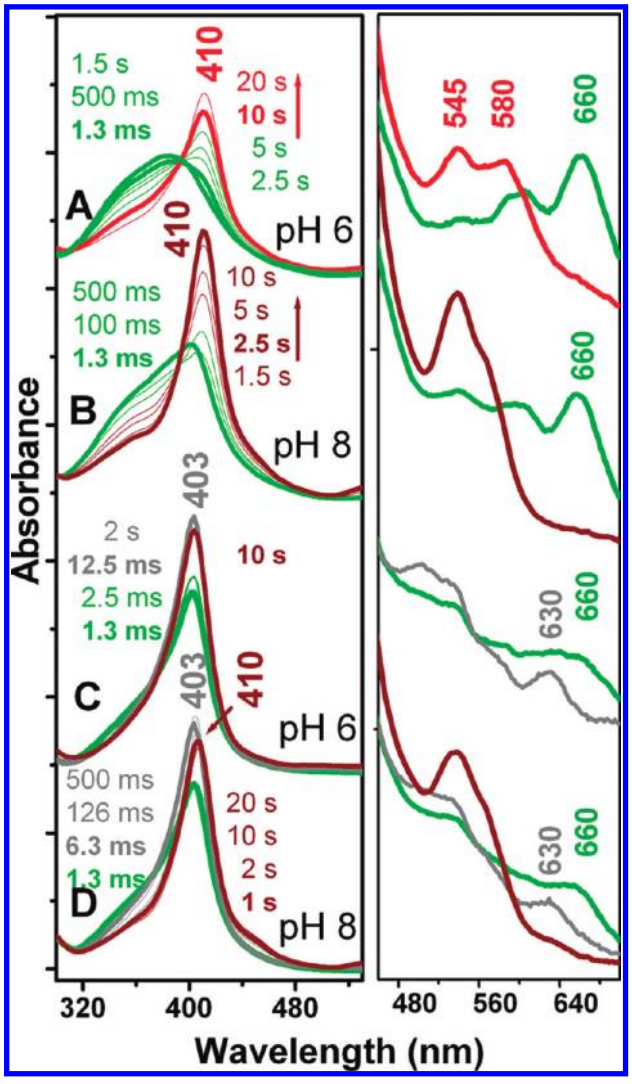

FIGURE 9: Rapid-scan electronic absorption spectra of the peroxidase-like reaction of the preformed [Fe^{IV}=O Por$^{\bullet}$]$^{+}$ intermediate of NP2 with histamine (A and B) and norepinephrine (C and D) at two pH values. Only representative spectra are shown, and the spectrum labeled 1.3 ms represents the first spectrum obtained upon reaction of the preformed [Fe^{IV}=O Por$^{\bullet}$]$^{+}$ species with each substrate. The experiments were performed as described in the legends of Figures 7 and 8. Final samples concentrations were 5, 10, and 25 μM for NP2, peroxyacetic acid, and histamine or norepinephrine, respectively. Experimental conditions are further described in Materials and Methods.

norepinephrine to NP2 at high pH. The NMR spectra of the low-spin complexes with norepinephrine or *n*-butylamine were also very similar (Figures S8−S12 of the Supporting Information); essentially all of the heme resonances could be assigned, but those with *n*-butylamine (but not norepinephrine) as the ligand showed significant chemical exchange at higher temperatures. Addition of catechol or BHA to NP2 at pH* 7 (pH* denotes the pH uncorrected for the deuterium isotope effect) or higher was shown to give high-spin NMR spectra identical to that of the ligand-free protein and to give high-spin EPR spectra identical to that of the ligand-free protein (Figure S4B of the Supporting Information).

DISCUSSION

Magnetic Properties of the [Fe^{IV}=O Por$^{\bullet}$]$^{+}$ *and* [Fe^{IV}=O Por](Tyr$^{\bullet}$) *Intermediates*. We have identified the electronic structure of the intermediates formed by the reaction of NP2 in its ferric oxidation state with hydrogen peroxide and peroxyacetic acid by using EPR spectroscopy. The complementary information obtained from EPR and stopped-flow electronic absorption studies allowed us to discriminate three intermediates in the peroxidase-like reaction of NP2, which are the [Fe^{IV}=O Por$^{\bullet}$]$^{+}$, [Fe^{IV}=O Por](Tyr$^{\bullet}$), and [Fe^{IV}=O Por] (Compound II) species. A remarkable pH dependence of the equilibrium among these species was observed. Specifically, [Fe^{IV}=O Por$^{\bullet}$]$^{+}$ was the stable and predominant intermediate formed at pH <7, as shown by both the EPR (Figure 1A, green trace) and the stopped-flow (Figure 5A, green trace) experiments. The 9 GHz EPR spectrum of the [Fe^{IV}=O Por$^{\bullet}$]$^{+}$ intermediate at pH <7 agreed well with that expected for a porphyrin radical in a strong ferromagnetic exchange interaction with the ferryl heme iron. Such a magnetic interaction has been exclusively observed in iron porphyrin model complexes with bulky *meso* substituents (*27*). There is no precedent for strong ferromagnetic exchange coupling for the [Fe^{IV}=O Por$^{\bullet}$]$^{+}$ intermediates of catalases or peroxidases (reviewed in ref *45*). At pH ≥ 7, the effective *g* values determined from the EPR spectrum of the [Fe^{IV}=O Por$^{\bullet}$]$^{+}$ intermediate of NP2 were consistent with a porphyrin radical with weaker ferromagnetic exchange coupling to the ferryl moiety (Figure 1B), which hence results in a spectrum similar to that of the [Fe^{IV}=O Por$^{\bullet}$]$^{+}$ species in ascorbate peroxidase (*46*).

An additional pH-induced and most probably correlated effect was the identification of the [Fe^{IV}=O Por](Tyr38$^{\bullet}$) species, formed after the [Fe^{IV}=O Por$^{\bullet}$]$^{+}$ intermediate. Both signals contributed to the EPR spectrum of NP2 at pH ≥ 7 (see Figure 1B), with a higher yield of the [Fe^{IV}=O Por](Tyr38$^{\bullet}$) species at basic pH. It is interesting that the formation of only the [Fe^{IV}=O Por$^{\bullet}$]$^{+}$ species at low pH and the equilibrium between the [Fe^{IV}=O Por$^{\bullet}$]$^{+}$ species and a [Fe^{IV}=O Por](Tyr38$^{\bullet}$) radical species at high pH in NP2 is reminiscent of the situation reported for one of the isoforms of turnip peroxidase (TP7) from *Brassicsa napus* roots (*47*). In the latter, the observed pH-induced change in the strength of the ferromagnetic exchange coupling interaction of the porphyrin radical was less drastic (see Figure 3 of ref *47*), because, as mentioned before, only the weak type of ferromagnetic exchange interaction occurs in the more planar hemes of peroxidases. Another difference between NP2 and TP7 is the fact that the EPR signal of the Tyr$^{\bullet}$ in TP7 did not show the broad signal that results from the exchange coupling interaction observed for the [Fe^{IV}=O Por](Tyr$^{\bullet}$) intermediate in NP2 (Figure 1D). The proposed site for the Tyr radical in TP7 is not in such close contact with the heme as in the case of NP2; i.e., it is within the second coordination sphere of the heme.

The fact that the [Fe^{IV}=O Por](Tyr$^{\bullet}$) species of NP2 was not detected at pH <7 may be explained by a significant change in the midpoint potential of the [Fe^{IV}=O Por$^{\bullet}$]$^{+}$ species that makes unfavorable the intramolecular electron transfer between Tyr38 and the porphyrin at low pH, or by the absence of the H-bonding interaction between Tyr38 and the heme propionate-7 (which would also modulate the oxidation potential of the Tyr), or most probably by both. The possibility of a change in the midpoint potential of the heme with a pH shift would agree well with the observed weakening of the exchange coupling of the [Fe^{IV}=O Por$^{\bullet}$]$^{+}$ species (see above). The absence of the H-bond of Tyr38 to the propionate at pH <7 agrees well with the crystal structure of the aqua complex of NP2 at pH 6.5, in which the distance between the phenolic oxygen of Tyr38 and the carboxylic group of propionate-7 is too long for a hydrogen bond (see Figure 2A).

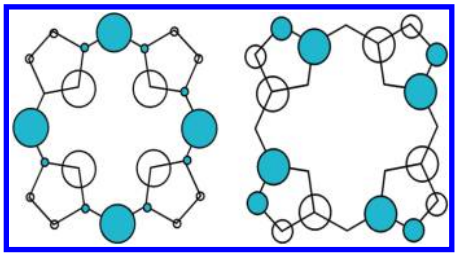

FIGURE 10: Electron density distribution in the two porphyrin orbitals that could be the HOMO of the porphyrin π-system and could thus exist as π-radicals for Compound I states of heme proteins: (left) $3a_{2u}(\pi)$ orbital and (right) $1a_{1u}(\pi)$ orbital.

Another interesting finding in this work concerns Tyr85, the only substitute for the radical site that formed exclusively when the naturally occurring site (Tyr38) was suppressed by the Y38F mutation. Moreover, the double Tyr mutation that suppressed both the primary and secondary radical sites in NP2 (Y38F/Y85F double mutant) demonstrates that none of the other nine Tyr residues can become an adventitious radical site. These results indicate that NP2 has two well-defined Tyr sites but only Tyr38 is the one stabilized in the native protein. This site could be playing the role of alternative [Fe^{IV}=O Por](Tyr$^{\bullet}$) intermediate for the peroxidase-like function of the protein. The situation is relevant for an improved understanding of the cases of tyrosyl and tryptophanyl radical intermediates in PGHS (*4*) and KatGs (*5*, *48*−*50*), respectively. In particular, recent studies of isoforms 1 and 2 of human PGHS showed that Tyr504 is an alternative site for the [Fe^{IV}=O Por](Tyr385$^{\bullet}$) species (*4*). It has been proposed that Tyr504 enhances the cyclooxygenation efficiency of PGHS, while Tyr385 is the radical site for the peroxidase reaction with arachidonic acid. In the case of the bifunctional catalase-peroxidases, a unique site (Trp106) for the formation of the neutral and H-bonded Trp$^{\bullet}$ was identified in the *Synechocystis* KatG (*48*, *49*). In *B. pseudomallei* KatG, the Trp at the position equivalent to that of *Synechocystis* KatG becomes the unique alternative site that stabilizes the Trp$^{\bullet}$ only when the three primary sites are suppressed by the triple mutant, W330F/W139F/W153F (*50*).

Role of Heme Ruffling in Determining the Strength of the Exchange Coupling Interaction between the Porphyrin Radical and the Fe^{IV}=O Species. The strong ferromagnetic coupling of the porphyrin radical in the [Fe^{IV}=O Por$^{\bullet}$]$^{+}$ species observed in NP2 at low pH (Figure 1A) is atypical of heme peroxidases. The hemes in nitrophorins are the most ruffled among heme proteins containing noncovalently attached heme *b* as active sites (see below), whereas the hemes in peroxidases are relatively planar (*51*−*58*). The distortion from planarity in hemes, i.e., the ruffling, arises from the alternate raising and lowering of the *meso* carbons, which leads to a rotation of the pyrrole rings about the Fe−N bonds. The pH-dependent change in the strength of the ferromagnetic coupling interaction of the porphyrin radical in NP2, not observed in peroxidases, could then be due to changes in the degree of heme ruffling in nitrophorins. Ruffling is believed to be related to the water molecules and/or Leu residues on the distal side of the heme, by the orientation of the His57 imidazole plane, and by the "belt" of mainly aromatic residues that surround the heme (*8*). The double mutation of Leu122 and Leu132 to Val on the distal side results in a less ruffled heme (*12*) (PDB entry 1PM1). Modifications of the H-bonding interactions to the heme propionates could also influence the ruffling. The crystal structure of NP2 at pH 7.7 (PDB entry 1EUO) shows that Tyr85 can form an H-bond to the carboxyl group of propionate-6 via a water molecule [water244 (see Figure 2, bottom)]. The EPR spectrum of the [Fe^{IV}=O Por$^{\bullet}$]$^{+}$ species in NP2 changed to one that agrees well with a weaker exchange coupling interaction when the H-bond interaction was suppressed by means of the Y85F mutation (see Figure 4B). This effect is also in line with the observation that in the nitrophorin isoform (NP4) containing a less ruffled heme, the residue at the position equivalent to Tyr85 in NP2 is not conserved.

As mentioned before, the nitrophorins are the most ruffled heme proteins that contain noncovalently attached heme *b* (*11*, *12*, *14*−*20*). Ruffling of the heme leads to overlap of the p_{π} orbitals of the heme nitrogens with the d_{xy} orbital of the metal, such that electronic interaction between the porphyrin $a_{2u}(\pi)$ orbital and the metal d_{xy} orbital becomes allowed (*59*). Thus, ruffling helps to stabilize the $(d_{xz},d_{yz})^4(d_{xy})^1$ electronic ground state of low-spin d^5 ferrihemes, as we have reported in detail for model ferriheme complexes (*59*−*64*), and recently in the cyanide complexes of the nitrophorins (*39*, *65*, *66*). We have also hypothesized that this stabilization is present in the NO adduct of NP2, which would facilitate NO dissociation by preventing the transfer of an electron from NO$^{\bullet}$ to Fe(III), because of orbital orthogonality (*9*, *10*). The same stabilization could hold true for the low-spin d^4 Fe^{IV}=O state, where two possible electron configurations can exist for the low-spin (S = 1) case: the more expected $(d_{xy})^2(d_{xz},d_{yz})^2$ or d_{π}^2 configuration and also the possible $(d_{xz},d_{yz})^3(d_{xy})^1$ or $d_{\pi}^3d_{xy}^1$ electron configuration. The first would, like the $(d_{xy})^2(d_{xz},d_{yz})^3$ configuration of low-spin d^5, be expected to exist when the heme is planar, while the second, like the $(d_{xz},d_{yz})^4(d_{xy})^1$ configuration of low-spin d^5, would be expected to exist when the heme is ruffled (*59*). Thus, a low-spin d^5 Fe(III) complex of a ruffled heme has strong bonding interaction between the (filled) $a_{2u}(\pi)$ orbital and the half-filled d_{xy} orbital that leads to large spin delocalization to the nitrogens and *meso* carbons by porphyrin → Fe π donation (*59*). In contrast, the two parallel-spin electrons, in the metal d_{xy} and one of the d_{π} orbitals, will lead to an antibonding interaction with the unpaired electron in the π-system of the porphyrin in the $a_{2u}(\pi)$ orbital with spin parallel to the two metal electrons. This will produce strong ferromagnetic coupling because the porphyrin $a_{2u}(\pi)$ orbital has large coefficients on the porphyrin nitrogens that match the symmetry of the d_{xy} orbital (see Figure 10). In contrast, if the porphyrin ring is flat, then neither of the two potential HOMOs, $a_{2u}(\pi)$ or $a_{1u}(\pi)$, has the proper symmetry to interact with either the d_{xy} or d_{π} orbitals of the metal. Thus, ferromagnetic coupling with a porphyrin radical will be weak, and in principle, it would not matter which of these orbitals holds the unpaired electron, although the nodes of the $a_{1u}(\pi)$ orbital at the porphyrin nitrogens mean that there would be less repulsion between porphyrin and metal electrons if this orbital were used. As it turns out, the [Fe^{IV}=O Por$^{\bullet}$]$^{+}$ species observed for the peroxidases and catalases typically have the electron hole in the $a_{1u}(\pi)$ orbital (*67*) (Figure 10), while most model heme [Fe^{IV}=O Por$^{\bullet}$]$^{+}$ radicals have the electron hole in the $a_{2u}(\pi)$ orbital (*24*−*27*). We propose that the $a_{2u}(\pi)$ radical typically observed for high-valent tetraphenylporphyrins is probably a result of ruffling of the porphyrin ring, rather than being a result of the presence of electron-withdrawing substituents on the phenyl rings of tetraphenylporphyrins as previously proposed (*34*). Tetramesitylporphyriniron(III) complexes are well-known to be ruffled, for example (*9*, *68*). In the case of 5-(2-chloro-6-nitrophenyl)-10,15,20-tris(2,6-dichlorophenyl)porphyrinato iron^{IV}=O and 5-(2,6-dinitrophenyl)-10,15,20-tris(2,6-dichlorophenyl)porphyrinato iron^{IV}=O (*34*),

the 2-chloro-6-nitro and 2,6-dinitro substituents were undoubtedly too bulky to permit ruffling, thus making these two complexes unique model hemes in having significant $a_{1u}(\pi)$ radical character. The $a_{1u}(\pi)$ radical complexes of Ayougou et al. (*28*) and Fujii et al. (*27*) are also likely forced to be planar (or saddled) by methyl substituents on one β-pyrrole position of each pyrrole ring, while the porpholactones of Weiss, Gold, Trautwein, et al. (*34*), although based on the same tetramesityl- or tetrakis(2,6-dichlorophenyl)porphyrin ring structure, simply have a different π-system, which appears to be stabilized as the $a_{1u}(\pi)$ form of the $[Fe^{IV}{=}O\ Por^{\bullet}]^{+}$ species.

In comparison to the more hindered of the model hemes studied by Fujii et al. (*27*) and Weiss, Gold, Trautwein, et al. (*27*, *34*), the hemes of the nitrophorins are forced to ruffle because of crowding by "distal pocket" and "belt" protein side chains (R. E. Berry, A. Amoia, A. Weichsel, T. K. Shokhireva, M. N. Shokhirev, W. J. Golden, H. Zhang, W. R. Montfort, and F. A. Walker, manuscript to be submitted). These heme proteins are seen to ruffle in all available crystal structures (*11*, *12*, *14*−*20*). In this work, we have found that the $[Fe^{IV}{=}O\ Por^{\bullet}]^{+}$ species formed in NP2 at pH <7 is an $a_{2u}(\pi)$ radical state with strong ferromagnetic coupling, while at pH ≥ 7, the $a_{1u}(\pi)$ radical state is observed. Thus, it is important to identify the origin of such a pH-dependent switch in the strength of ferromagnetic coupling. This will require crystallization of NP2 at pH ≥ 8 and determination of the three-dimensional structure.

Peroxidase-like Reaction of NP2. The crystal structures of NP2 currently available show that the heme environment is substantially different from that of peroxidases (Figure 2, top). NP2 lacks the key residues of the heme distal and proximal sides that are involved in the formation of the high-valent $Fe^{IV}{=}O$ species through the O−O bond cleavage of the bound hydrogen peroxide, described as the "push−pull" effect (*69*). Specifically, the Asp that acts as a H-bond acceptor from the $N^{\delta}H$ atom of the His axial ligand of peroxidases makes the His imidazole nitrogen a better electron pair donor and thereby provides the "push" effect on the proximal side. The distal His of peroxidases serves as a proton donor to the peroxide, and the negatively charged Arg may polarize the O−O bond in the "pull" effect on the distal side (*70*) [although recent work suggests the Arg may be more important in stabilizing the ferryl oxo group (*71*, *72*)]. Other enzymes, such as cytochromes P450, can do the cleavage of the O−O bond with only the push effect of the axial thiolate, given that they lack the His and Arg on the heme distal side (ref *69* and references cited therein). In the case of NP2, there is no negatively charged group that can accept the H-bond from the histidine axial ligand to enhance the push effect, yet the crystal structure shows a water molecule [water181 (see Figure 2)] at a very suitable position for the water O to accept a H-bond from the $N^{\delta}H$ group of His57 (axial ligand), which would certainly be weaker than that of peroxidases. This water molecule is in turn an H-bond donor to the carbonyl O of Asn68, which might strengthen its acceptance of the H-bond from the $N^{\delta}H$ group of His57 [it should be noted that NP1 and NP4 have Asp70 in place of Asn68, yet the H_2O molecule is conserved in those structures over the pH range of 7.7−5.6 (*15*−*20*)]. This slight histidinate character of the axial ligand in NP2, due to the weak H-bond from His57 to the water molecule and to Asn68, may also explain the observed lower stability of the $[Fe^{IV}{=}O\ Por^{\bullet}]^{+}$ species formed upon reaction with H_2O_2, in particular at pH 6 (see Figure 6).

The higher stability of the $[Fe^{IV}{=}O\ Por^{\bullet}]^{+}$ intermediate, as well as the much higher levels of peroxidase activity obtained with peroxyacetic acid (Table 1), may be explained by the possible donation of a hydrogen bond from a protonated heme propionate to the carbonyl group of bound PAA, which could speed the heterolytic breaking of the O−O bond to form the Compound I species. In contrast, H_2O_2 could not participate in such H-bonding from a heme propionate, and this may slow the heterolytic cleavage of the O−O bond.

Another consequence of the structural differences in the heme active site of NP2 and peroxidases is that the binding site for aromatic molecules, such as benzohydroxamic acid, that has been identified in peroxidases (ref *32* and references cited therein) cannot exist in NP2, because of the considerable differences on the distal side (see above). Consequently, the fast and efficient reaction of the $[Fe^{IV}{=}O\ Por^{\bullet}]^{+}$ intermediate of NP2 with BHA and norepinephrine shown in this work (see Figures 7−9) is most possibly due to a relatively accessible heme distal side, if one considers that histamine and norepinephrine can access and directly bind to the heme ferric iron, albeit using opposite ends of the two molecules (Supporting Information). Another interesting finding in the peroxidase-like reaction of NP2 was the high reactivity of the $[Fe^{IV}{=}O\ Por]$ (Compound II) intermediate with all three substrates. The exception was histamine at pH 6, in which the characteristic absorption spectrum of the $[Fe^{IV}{=}O\ Por]$ species (Figure 9A, red trace) was clearly detected within 10 s and did not further react with the substrate at low pH. (However, this may be aided by protonation of the imidazole nitrogen of histamine at pH 6.)

Peroxidases show differences in stability, reactivity, and magnetic properties of their high-valent intermediates, but the correlation between them is not well understood. For example, the crystal structures of ascorbate and lignin peroxidases did not reveal substantial differences that would explain the differences in the exchange coupling interaction of their porphyrin radicals, as shown by the EPR spectra of their $[Fe^{IV}{=}O\ Por^{\bullet}]^{+}$ intermediates (reviewed in ref *45*). In addition, the $[Fe^{IV}{=}O\ Por^{\bullet}]^{+}$ species in lignin peroxidase is short-lived, as is the subsequent $[Fe^{IV}{=}O\ Por](Trp^{\bullet})$ intermediate (*38*), in contrast to the relatively stable $[Fe^{IV}{=}O\ Por^{\bullet}]^{+}$ species of ascorbate peroxidase (*46*). Our findings with NP2 open the possibility of analyzing the factors that determine the reactivity of the high-valent intermediates under conditions that better replicate those of mono- and bifunctional peroxidases, and catalases (substrate access, heme environment, Tyr or Trp sites for alternative reactive intermediates, and magnetic properties of the heme), compared to those of the model complexes.

Peroxidase-like Function of Nitrophorins: A Complementary Biological Role for the Release of NO and Binding of Histamine at Physiological pH?. The significant levels of peroxidase activity of NP2, and the possibility of trapping and characterizing the reactive intermediates of the peroxidase-like reaction of the protein, led us to inspect the kinetics of a putative reaction of NP2 with histamine and norepinephrine as a function of pH (see Figure 11). The stopped-flow experiments clearly showed a fast reaction of NP2 with norepinephrine (see Figure 9C,D). Accordingly, when the preformed $[Fe^{IV}{=}O\ Por^{\bullet}]^{+}$ species of NP2 reacts with norepinephrine, the protein cycles back to the ferric (resting) state within ~15 ms (see Figure 9). Another remarkable difference of this reaction is the slow binding of norepinephrine, which occurs exclusively at basic pH. Accordingly, a further conversion of the ferric high-spin state [which results from the reaction with norepinephrine (Figure 9D, gray trace)] to that of the NP2−norepinephrine complex

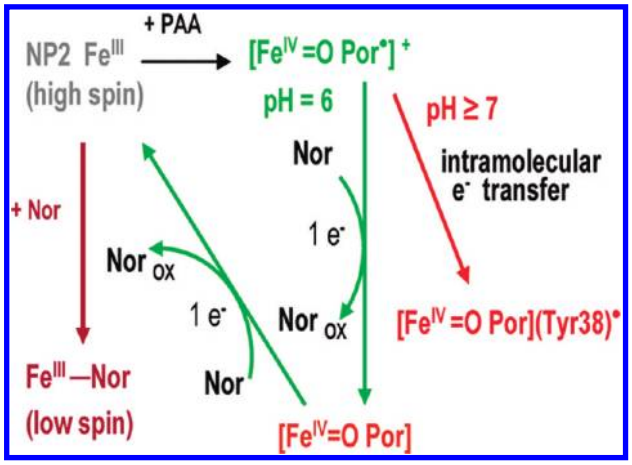

FIGURE 11: Schematic representation of the intermediates formed upon reaction of nitrophorin 2 (NP2) with peroxyacetic acid (PAA) as identified by EPR spectroscopy characterization (Figures 1A,B and 3). The proposed peroxidase-like reaction of NP2 with norepinephrine as a substrate is based on the kinetic studies (Figure 9C,D and Table 3).

[ferric low-spin (Figure 9D, dark red trace)] was observed exclusively at pH 8. The reaction with histamine at pH 8 was considerably slower than with norepinephrine, and the resulting species was the ferric NP2−histamine−imidazole (low-spin) complex (Figure 9B, dark red trace). Accordingly, a selective and more efficient peroxidase-like reaction of NP2 with norepinephrine is expected to occur if both histamine and norepinephrine are present in the host blood. Norepinephrine is secreted directly into the blood by the adrenal glands in response to a stress such as pain or anxiety, in a hormonelike action. The effect of norepinephrine is then to increase heart rate and blood pressure and to open up the air passages to the lungs of the host. In contrast, histamine is part of the immune response of the host. The biological implications of our findings are that in the presence of hydrogen peroxide, the peroxidase-like reaction of NP2 with histamine and norepinephrine as substrates may be by far a more efficient strategy for counteracting the host response to the injection of the insect saliva. Effectively, the fast reaction of NP2 at physiological pH would facilitate the deactivation of a higher number of norepinephrine and histamine molecules per protein molecule, as compared to the one-to-one capturing effect (binding to the heme iron) by the ferric protein. Hence, we conclude that the peroxidase-like activity of NP2 and its NO binding and release and histamine binding capabilities are the key protein functions that are biologically relevant in nitrophorins.

CONCLUSIONS

We have identified and characterized the unprecedented peroxidase-like function of nitrophorin isoform 2. The specific activity measured with typical peroxidase substrates was comparable to that of the bifunctional peroxidases (KatGs). The complementary information obtained from EPR spectroscopy and stopped-flow electronic absorption studies allowed us to discriminate three intermediates, [Fe^{IV}=O Por$^{•}$]$^{+}$, [Fe^{IV}=O Por](Tyr$^{•}$), and [Fe^{IV}=O Por] (Compound II). The [Fe^{IV}=O Por$^{•}$]$^{+}$ species was predominant at pH <7 and exhibited a strong ferromagnetic exchange coupling of the porphyrin radical with the ferryl iron. The strong ferromagnetic interaction is unprecedented in heme peroxidases and catalases. Site-directed mutagenesis combined with EPR spectroscopy allowed us to identify an [Fe^{IV}=O Por](Tyr$^{•}$) species formed subsequent to the [Fe^{IV}=O Por$^{•}$]$^{+}$ species at pH ≥ 7, with the radical site being the Tyr residue (Tyr38) in a H-bonding interaction with heme propionate-7. The Y38F variant showed that when the naturally occurring radical site is suppressed, the Tyr residue (Tyr85) in an indirect H-bonding interaction with the other heme propionate is the only alternative radical site. On the basis of such peculiarities of the NP2 intermediates, the protein provides an excellent model system for studying and better understanding the more complex cases of other heme bifunctional enzymes such as PGHS and KatGs. The kinetic studies with NP2 revealed that the [Fe^{IV}=O Por$^{•}$]$^{+}$ species can react with both histamine and norepinephrine in a peroxidase-like manner. We propose that the efficient reaction of NP2 with norepinephrine at physiological pH is indicative of an alternative strategy for neutralizing the effect of norepinephrine, a molecule that is released into the bloodstream as a consequence of the insect bite. Hence, the nitrophorin behaves as a NO carrier when exposed to the acidic pH of the insect saliva. If exposed to the higher pH of the tissues and the capillaries, NP2 in its ferric state will either capture histamine or, in the presence of hydrogen peroxide, efficiently inactivate norepinephrine through a peroxidase-like reaction.

ACKNOWLEDGMENT

The Fe(III) (tmtmp) triflate model heme complex was a kind gift from Professor Avram Gold (University of North Carolina, Chapel Hill, NC).

SUPPORTING INFORMATION AVAILABLE

Additional optical and EPR spectra discussed in the text and NMR spectra of norepinephrine and *n*-butylamine complexes of NP2. This material is available free of charge via the Internet at http://pubs.acs.org.

REFERENCES

1. Singh, R., Wiseman, B., Deemagarn, T., Donald, L. J., Duckworth, H. W., Carpena, X., Fita, I., and Loewen, P. C. (2004) Catalase-peroxidases (KatG) exhibit NADH oxidase activity. *J. Biol. Chem. 279*, 43098–43106.
2. Carpena, X., Wiseman, B., Deemagarn, T., Singh, R., Switala, J., Ivancich, A., Fita, I., and Loewen, P. C. (2005) A molecular switch and electronic circuit modulate catalase activity in catalase-peroxidases. *EMBO Rep. 6*, 1156–1162.
3. Deemagarn, T., Wiseman, B., Carpena, X., Ivancich, A., Fita, I., and Loewen, P. C. (2007) Two alternative substrate paths for compound I formation and reduction in catalase-peroxidase KatG from *Burkholderia pseudomallei*. *Proteins 66*, 219–228.
4. Tsai, A.-L., and Kulmacz, R. J. (2010) Prostaglandin H synthase: Resolved and unresolved mechanistic issues. *Arch. Biochem. Biophys. 493*, 103–124.
5. Singh, R., Switala, J., Loewen, P. C., and Ivancich, A. (2007) Two [Fe(IV)=O Trp$^{•}$] intermediates in *M. tuberculosis* catalase-peroxidase discriminated by multifrequency (9−285 GHz) EPR spectroscopy: Reactivity toward isoniazid. *J. Am. Chem. Soc. 129*, 15954–15963.
6. Zhao, X., Suarez, J., Khajo, A., Yu, S., Metlistsky, L., and Magliozzo, R. (2010) A Radical on the Met-Tyr-Trp Modification Required for Catalase Activity in Catalase-Peroxidase Is Established by Isotopic Labeling and Site-Directed Mutagenesis. *J. Am. Chem. Soc. 131*, 8268–8269.
7. Walker, F. A., Ribeiro, J. M. C., and Montfort, W. R. (1999) Novel NO-liberating heme proteins from the saliva of blood-sucking insects. In Metal Ions in Biological Systems, Vol. 36, Interrelations between Free Radicals and Metal Ions in Life Processes (Sigel, H., and Sigel, A., Eds.) pp 619−661, Marcel Dekker, New York.
8. Walker, F. A., and Montfort, W. R. (2001) Nitric oxide-releasing heme proteins from the saliva of the blood-sucking insect *Rhodnius prolixus*. In Advances in Inorganic Chemistry (Mauk, A. G., and Sykes, A. G., Eds.) Vol. 51, Chapter 5, pp 295−358, Academic Press, San Diego.

9. Walker, F. A. (2005) Nitric oxide interaction with insect nitrophorins, and thoughts on the electron configuration of the $\{FeNO\}^6$ complex. *J. Inorg. Biochem. 99*, 216–236.
10. Walker, F. A. (2008) Nitric oxide interaction with insect nitrophorins, and possibilities for the electron configuration of the $\{FeNO\}^6$ complex. In The Smallest Biomolecules: Diatomics and their Interactions with Heme Proteins (Ghosh, A., Ed.) pp 378−428, Elsevier B. V., Amsterdam.
11. Andersen, J. F., and Montfort, W. R. (2000) The crystal structure of nitrophorin 2. *J. Biol. Chem. 275*, 30496–30503.
12. Weichsel, A., Berry, R. E., Zhang, H., Walker, F. A., and Montfort, W. R. (1999−2002) PDB entries 1PEE, 1PM1, 1T68, 2A3F, 2ACP, 2AH7, 2AL0, 2ALL, 2AMM, 2ASN, 2EU7, 2HYS, and 2GTF available, manuscript in preparation.
13. Ribeiro, J. M. C., Hazzard, J. M. H., Nussenzveig, R., Champagne, D., and Walker, F. A. (1993) Reversible binding of nitric oxide by a salivary nitrosylheme protein from the blood sucking insect, *Rhodnius prolixus*. *Science 260*, 539–541.
14. Weichsel, A., Andersen, J. F., Champagne, D. E., Walker, F. A., and Montfort, W. R. (1998) Crystal structures of a nitric oxide transport protein from a blood-sucking insect. *Nat. Struct. Biol. 5*, 304–309.
15. Ding, X. D., Weichsel, A., Andersen, J. F., Shokhireva, T. K., Balfour, C., Pierik, A. J., Averill, B. A., Montfort, W. R., and Walker, F. A. (1999) Nitric oxide binding to the ferri- and ferroheme states of nitrophorin 1, a reversible NO-binding heme protein from the saliva of a blood-sucking insect, *Rhodnius prolixus*. *J. Am. Chem. Soc. 121*, 128–138.
16. Andersen, J. F., Weichsel, A., Balfour, C. A., Champagne, D. E., and Montfort, W. R. (1998) The crystal structure of nitrophorin 4 at 1.5 Å resolution: Transport of nitric oxide by a lipocalin-based heme protein. *Structure 6*, 1315–1327.
17. Weichsel, A., Andersen, J. F., Roberts, S. A., and Montfort, W. R. (2000) Nitric oxide binding to nitrophorin 4 induces complete distal pocket burial. *Nat. Struct. Biol. 7*, 551–554.
18. Roberts, S. A., Weichsel, A., Qiu, Y., Shelnutt, J. A., Walker, F. A., and Montfort, W. R. (2001) Ligand-induced heme ruffling and bent NO geometry in ultra-high resolution structures of nitrophorin 4. *Biochemistry 40*, 11327–11337.
19. Maes, E. M., Weichsel, A., Andersen, J. F., Shepley, D., and Montfort, W. R. (2004) Role of binding site loops in controlling nitric oxide release: Structure and kinetics of mutant forms of nitrophorin 4. *Biochemistry 43*, 6679–6690.
20. Maes, E. M., Roberts, S. A., Weichsel, A., and Montfort, W. R. (2005) Ultrahigh resolution structures of nitrophorin 4: Heme distortion in ferrous CO and NO complexes. *Biochemistry 44*, 12690–12699.
21. Ribeiro, J. M. C. (1996) Salivary thiol oxidase activity of *Rhodnius prolixus*. *Insect Biochem. Mol. Biol. 26*, 899–905.
22. Varma, S. D., and Devamanoharan, P. S. (1991) Hydrogen peroxide in human blood. *Free Radical Res. 14*, 125–131.
23. Ribeiro, J. M. C. (1998) *Rhodnius prolixus* salivary nitrophorins display heme-peroxidase activity. *Insect Biochem. Mol. Biol. 28*, 1051–1057.
24. Bill, E., Ding, X.-Q., Bominaar, E. L., Trautwein, A. X., Winkler, H., Mandon, D., Weiss, R., Gold, A., Jayaraj, K., Hatfield, W. E., and Kirk, M. L. (1990) Evidence for variable metal-radical spin coupling in oxoferrylporphyrin cation radical complexes. *Eur. J. Biochem. 188*, 665–672.
25. Mandon, D., Weiss, R., Jayaraj, K., Gold, A., Terner, J., Bill, E., and Trautwein, A. X. (1992) Models for peroxidase compound I: Generation and spectroscopic characterization of new oxoferryl porphyrin π cation radical species. *Inorg. Chem. 31*, 4404–4409.
26. Jayaraj, K., Terner, J., Gold, A., Roberts, D. A., Austin, R. N., Mandon, D., Weiss, R., Bill, E., Müther, M., and Trautwein, A. X. (1996) Influence of meso substituents on electronic states of (oxoferryl)porphyrin π-cation radicals. *Inorg. Chem. 35*, 1632–1640.
27. Fujii, H., Yoshimura, T., and Kamada, H. (1996) ESR studies of A1u and A2u oxoiron(IV) porphyrin π-cation radical complexes. Spin coupling between ferryl iron and A1u/A2u orbitals. *Inorg. Chem. 35*, 2373–2377.
28. Ayougou, K., Mandon, D., Fischer, J., Weiss, R., Müther, M., Schünemann, V., Trautwein, A. X., Bill, E., Terner, J., Jayaraj, K., Gold, A., and Austin, R. N. (1996) Molecular structure of the chloroiron(III) derivative of the *meso*-unsubstituted 2,7,12,17-tetramethyl-3,8,13,18-tetramesitylporphyrin and weak ferromagnetic exchange interactions in the A_{1u} oxoiron(IV) porphyrin π radical cation complex. *Chem.—Eur. J. 2*, 1159–1163.
29. Shokhireva, T. Kh., Berry, R. E., Uno, E., Balfour, C. A., Zhang, H., and Walker, F. A. (2003) Electrochemical and NMR spectroscopic studies of distal pocket mutants of nitrophorin 2: Stability, structure and dynamics of axial ligand complexes. *Proc. Natl. Acad. Sci. U.S.A. 100*, 3778–3783.
30. Berry, R. E., Shokhireva, T. K., Filippov, I., Shokhirev, M. N., Zhang, H., and Walker, F. A. (2007) The effect of the N-terminus on heme cavity structure, ligand equilibrium and rate constants, and reduction potentials of nitrophorin 2 from *Rhodnius prolixus*. *Biochemistry 46*, 6830–6843.
31. Champagne, D. E., Nussenzveig, R. H., and Ribeiro, J. M. C. (1995) Purification, partial characterization, and cloning of nitric oxide-carrying heme proteins (nitrophorins) from salivary glands of the blood-sucking insect *Rhodnius prolixus*. *J. Biol. Chem. 270*, 8691–8695.
32. Dunford, B. H. (1999) in Heme Peroxidases, Wiley-VCH, New York.
33. Singh, R., Wiseman, B., Deemagarn, T., Jha, V., Switala, J., and Loewen, P. C. (2008) Comparative study of catalase-peroxidases (KatGs). *Arch. Biochem. Biophys. 471*, 207–214.
34. Jayaraj, K., Gold, A., Austin, R. N., Ball, L. M., Terner, J., Mandon, D., Weiss, R., Fischer, J., DeCian, A., Bill, E., Müther, M., Schünemann, V., and Trautwein, A. X. (1997) Compound I and compound II analogues from porpholactones. *Inorg. Chem. 36*, 4555–4566.
35. Ivancich, A., Dorlet, P., Goodin, D. B., and Un, S. (2001) Multifrequency high-field EPR study of the tryptophanyl and tyrosyl radical intermediates in wild-type and the W191G mutant of cytochrome c peroxidase. *J. Am. Chem. Soc. 123*, 5050–5058.
36. Fielding, A. J., Singh, R., Boscolo, B., Ghibaudi, E. M., and Ivancich, A. (2008) Intramolecular electron transfer versus substrate oxidation in lactoperoxidase: Investigation of radical intermediates by stopped-flow absorption spectrophotometry and (9−285 GHz) electron paramagnetic resonance spectroscopy. *Biochemistry 47*, 9781–9792.
37. Ivancich, A., Jouve, H. M., Sartot, B., and Gaillard, J. (1997) EPR investigation of compound I in *Proteus mirabilis* and bovine liver catalases: Formation of porphyrin and tyrosyl radical intermediates. *Biochemistry 36*, 9356–9364.
38. Smith, A. T., Doyle, W. A., Dorlet, P., and Ivancich, A. (2009) Spectroscopic evidence for an engineered catalytically-active Trp radical that recreates the unique reactivity of lignin peroxidase. *Proc. Natl. Acad. Sci. U.S.A. 106*, 16084–16089.
39. Yang, F., Knipp, M., Berry, R. E., Shokhireva, T. K., Zhang, H., and Walker, F. A. (2009) ^1H and ^{13}C NMR spectroscopic studies of the ferriheme resonances of the low-spin imidazole, histamine and cyanide complexes of *wt* nitrophorin 2 and NP2(V24E) as a function of pH. *J. Biol. Inorg. Chem. 14*, 1077–1095.
40. Nagasawa, H. T., DeMaster, E. G., Redfern, B., Shirota, F. N., and Goon, D. J. W. (1990) Evidence for nitroxyl in the catalase-mediated bioactivation of the alcohol deterrent agent cyanamide. *J. Med. Chem. 33*, 3120–3122.
41. Nagasawa, H. T., Lee, M. J. C., Kwon, C.-H., Shirota, F. N., and DeMaster, E. G. (1992) An N-hydroxylated derivative of cyanamide that inhibits yeast aldehyde dehydrogenase. *Alcohol 9*, 349–353.
42. King, S. B. (2003) The nitric oxide producing reactions of hydroxyurea. *Curr. Med. Chem. 10*, 437–452.
43. Berry, R. E., Shokhirev, M. N., Ho, A. Y. W., Yang, F., Shokhireva, T. K., Zhang, H., Weichsel, A., Montfort, W. R., and Walker, F. A. (2009) The effect of mutation of carboxylate side-chain amino acids near the heme on the midpoint potentials and ligand binding constants of nitrophorin 2 and its NO, histamine and imidazole complexes. *J. Am. Chem. Soc. 131*, 2313–2327.
44. Astashkin, A. V., Raitsimring, A. M., and Walker, F. A. (1999) Two- and four-pulse ESEEM studies of the heme binding center of a low-spin ferriheme protein: The importance of a multi-frequency approach. *Chem. Phys. Lett. 306*, 9–17.
45. Smulevich, G., Feis, A., Howes, B. D., and Ivancich, A. (2010) Structure-function relationships in heme peroxidases: New insights from electronic absorption, resonance Raman and multifrequency electron paramagnetic resonance spectroscopies. In The Handbook of Porphyrin Science (Kadish, K. M., Smith, K. M., and Guilard, R., Eds.) Vol. 6, Chapter 31, pp 367−453, World Scientific, Hackensack, NJ.
46. Patterson, W. R., Poulos, T. L., and Goodin, D. B. (1995) Identification of a porphyrin π-cation radical in ascorbate peroxidase Compound I. *Biochemistry 34*, 4342–4345.
47. Ivancich, A., Mazza, G., and Desbois, A. (2001) Comparative electron paramagnetic resonance study of radical intermediates in turnip peroxidase isozymes. *Biochemistry 40*, 6860–6866.
48. Ivancich, A., Jakopitsch, C., Auer, M., Un, S., and Obinger, C. (2003) Protein-based radicals in the catalase-peroxidase of *Synechocystis* PCC6803: A multifrequency EPR investigation of wild-type and variants on the environment of the heme active site. *J. Am. Chem. Soc. 125*, 14093–14102.

49. Jakopitsch, C., Obinger, C., Un, S., and Ivancich, A. (2006) Identification of Trp106 as the tryptophanyl radical intermediate in *Synechocystis* PCC6803 catalase-peroxidase by multifrequency electron paramagnetic resonance spectroscopy. *J. Inorg. Biochem. 100*, 1091–1099.
50. Colin, J., Wiseman, B., Switala, J., Loewen, P. C., and Ivancich, A. (2009) Distinct role of specific tryptophans in facilitating electron transfer or as [Fe(IV)═O Trp$^{\bullet}$] intermediates in the peroxidase reaction of *Bulkholderia pseudomallei* catalase-peroxidase: A multifrequency EPR spectroscopy investigation. *J. Am. Chem. Soc. 131*, 8557–8563.
51. Poulos, T. L., Freer, S. T., Alden, R. A., Edwards, S. L., Skogland, U., Takio, K., Eriksson, B., Xuong, N., Yonetani, T., and Kraut, J. (1980) The crystal structure of cytochrome c peroxidase. *J. Biol. Chem. 255*, 575–580.
52. Zheng, J., and Fenna, R. E. (1992) X-ray crystal structure of canine myeloperoxidase at 3 Å resolution. *J. Mol. Biol. 226*, 185–207.
53. Kunishima, N., Fukuyama, K., Matsubara, H., Hatanaka, H., Shibano, Y., and Amachi, T. (1994) Crystal structure of the fungal peroxidase from *Arthromyces ramosus* at 1.9 Å resolution: Structural comparisons with the lignin and cytochrome *c* peroxidases. *J. Mol. Biol. 235*, 331–344.
54. Gajhede, M., Schuller, D. J., Henriksen, A., Smith, A. T., and Poulos, T. L. (1997) Crystal structure of horseradish peroxidase C at 2.15 Å resolution. *Nat. Struct. Biol. 4*, 1032–1038.
55. Sharp, K. H., Mewies, M., Moody, P. C., and Raven, E. I. (2003) Crystal structure of the ascorbate peroxidase-ascorbate complex. *Nat. Struct. Biol. 10*, 303–307.
56. Bertrand, T., Eady, N. A., Jones, J. N., Jesmin, Nagy, J. M., Jamart-Grégoire, R., Raven, E. L., and Brown, K. A. (2004) Crystal structure of *Mycobacterium tuberculosis* catalase-peroxidase. *J. Biol. Chem. 279*, 38991–38999.
57. Singh, A. K., Singh, N., Sharma, S., Singh, S. R., Kaur, P., Bhushan, A., Srinivasan, A., and Singh, T. P. (2008) Crystal structure of lactoperoxidase at 2.4 Å resolution. *J. Mol. Biol. 376*, 1060–1075.
58. Singh, A. K., Kumar, R. P., Pandey, N., Singh, N., Sinha, M., Ghushan, A., Kaur, P., Sharma, S., and Singh, T. P. (2010) Mode of binding of the tuberculosis prodrug isoniazid to heme peroxidases. Binding studies and crystal structure of bovine lactoperoxidase with isoniazid at 2.7 Å resolution. *J. Biol. Chem. 285*, 1569–1576.
59. Safo, M. K., Walker, F. A., Raitsimring, A. M., Walters, W. P., Dolata, D. P., Debrunner, P. G., and Scheidt, W. R. (1994) Axial ligand orientation in iron(III) porphyrinates: Effect of axial π-acceptors. Characterization of the low-spin bis-pyridine complex $[Fe(TPP)(4\text{-}CNPy)_2]ClO_4$. *J. Am. Chem. Soc. 116*, 7760–7770.
60. Walker, F. A., Nasri, H., Turowska-Tyrk, I., Mohanrao, K., Watson, C. T., Shokhirev, N. V., Debrunner, P. G., and Scheidt, W. R. (1996) π-Acid ligands in iron(III) porphyrinates. Characterization of low-spin bis(*t*-butylisocyanide)(porphyrinato)iron(III) complexes having $(d_{xz},d_{yz})^4(d_{xy})^1$ ground states. *J. Am. Chem. Soc. 118*, 12109–12118.
61. Yatsunyk, L. A., and Walker, F. A. (2004) Structural, NMR and EPR studies of S = 1/2 and S = 3/2 Fe(III) bis-4-cyanopyridine complexes with dodecasubstituted porphyrins. *Inorg. Chem. 43*, 757–777.
62. Yatsunyk, L. A., and Walker, F. A. (2004) NMR and EPR spectroscopic and structural studies of low-spin $(d_{xz},d_{yz})^4(d_{xy})^1$ ground state Fe(III) bis-(*tert*-butylisocyanide) complexes of dodecasubstituted porphyrinates. *Inorg. Chem. 43*, 4341–4352.
63. Cai, S., Lichtenberger, D. L., and Walker, F. A. (2005) NMR and EPR studies of the bis-pyridine and bis-*t*-butylisocyanide complexes of iron(III) octaethylchlorin. *Inorg. Chem. 44*, 1890–1903.
64. Cai, S., Shokhireva, T. K., Lichtenberger, D. L., and Walker, F. A. (2006) NMR and EPR studies of chloroiron(III) tetraphenylchlorin and its complexes with imidazoles and pyridines of widely differing basicities. *Inorg. Chem. 45*, 3519–3531.
65. Shokhireva, T. K., Weichsel, A., Smith, K. M., Berry, R. E., Shokhirev, N. V., Balfour, C., Zhang, H., Montfort, W. R., and Walker, F. A. (2007) Assignment of the ferriheme resonances for low-spin complexes of nitrophorins 1 and 4 by ^1H and ^{13}C NMR spectroscopy: Comparison to structural data obtained from X-ray crystallography. *Inorg. Chem. 46*, 2041–2056.
66. Shokhireva, T. K., Berry, R. E., Shokhirev, N. V., Zhang, H., and Walker, F. A. (2008) Assignment of ferriheme resonances for high- and low-spin forms of the symmetrical hemin-reconstituted nitrophorins 1−4 by ^1H and ^{13}C NMR spectroscopy: The dynamics of heme ruffling deformations. *J. Biol. Inorg. Chem. 13*, 941–959.
67. Ivancich, A., Mazza, G., and Desbois, A. (2001) Comparative electron paramagnetic resonance study of radical intermediates in turnip peroxidase isozymes. *Biochemistry 40*, 6860–6866.
68. Safo, M. K., Gupta, G. P., Walker, F. A., and Scheidt, W. R. (1991) Models of the cytochromes *b*. Control of axial ligand orientation with a 'hindered' porphyrin system. *J. Am. Chem. Soc. 113*, 5497–5510.
69. Dawson, J. H. (1988) Probing structure-function relations in heme-containing oxygenases and peroxidases. *Science 240*, 433–439.
70. Poulos, T. L. (1987) Heme enzyme crystal structures. *Adv. Inorg. Biochem. 7*, 1–36.
71. Poulos, T. L. (2000) Peroxidase and Cytochrome P450 Structures. In The Porphyrin Handbook (Kadish, K. M., Smith, K. M., and Guilard, R., Eds.) Vol. 4, pp 189−218, Academic Press, San Diego.
72. Poulos, T. L. (2010) Thirty years of heme peroxidase structural biology. *Arch. Biochem. Biophys. 500*, 3–12.